Surface-electronic-structure information from bulk plasmon photoexcitation in free-electron metal films*

Peter J. Feibelman
Sandia Laboratories, Albuquerque, New Mexico 87115
(Received 19 May 1975)

Bulk-plasmon-photoexcitation (BPPE) phenomena (particularly the shapes of resonance peaks associated with standing-plasma-wave excitation) in thin free-electron-metal films are shown to be sensitive to surface electronic structure. A formalism is developed which permits the microscopic evaluation of corrections to the classical theory of the optical properties of a jellium solid, through first order in the wave vector of an incident electromagnetic wave. This formalism permits the evaluation of effects due to BPPE in both the ordinary optical as well as in the photoemissive properties of thin films, and moreover, allows one to determine their dependence on the forms of the one-electron surface potential barriers $V(z)$ at the two film surfaces. Theoretical results based on the random phase approximation (RPA) to a jellium film's dielectric response are compared to the photoyield data of Anderegg *et al.* taken on potassium films. The experimental BPPE resonance features are found to be considerably narrower than the theory predicts—for all the forms of $V(z)$ that were tried—casting some doubt on the RPA's ability to describe surface dielectric phenomena quantitatively. The asymmetry of Anderegg *et al.*'s films, i.e., the fact that their upper and lower film surfaces were inequivalent, is shown to require a partial reinterpretation of their data; in particular, their films were probably only about half as thick as they supposed. Moreover, the argument that leads to this conclusion also provides a simple explanation for the alternation of BPPE resonance peak strengths which appears to be a fairly systematic feature of their data. Directions for further experimental and theoretical work on BPPE phenomena are suggested.

I. INTRODUCTION

In this paper a new possibility is explored for obtaining information regarding the electronic structure of free-electron metal surfaces, specifically, the observation of bulk plasmon photoexcitation (BPPE) in free-electron metal films. In an infinite homogeneous dielectric medium, there is no coupling between transverse and longitudinal waves. Therefore, BPPE in a solid can occur only because of spatial inhomogeneities, either those associated with the discreteness of the solid's ion cores, or those associated with its surfaces. For free-electron metals, moreover, the spatial variation of the effective lattice potential is weak. Thus one would expect the strength of BPPE in such metals to be largely governed by the electronic structure of their surfaces.

The experimental situation in which BPPE should be easiest to observe was first proposed by Melnyk and Harrison[1] (in a paper henceforth referred to as MH), who pointed out that although the observable effects of BPPE are small for light incident on a semi-infinite sample, they may be strongly (resonantly) enhanced for a thin film of the same material at frequencies such that plasmon standing waves can be excited. MH's idea was subsequently confirmed, at least qualitatively, by Anderegg, Feuerbacher, and Fitton[2] (henceforth AFF) via measurements of photoelectric yield[3] versus photon frequency for thin ($\lesssim 100$ Å) potassium films. Specifically, in the photoyield data from each of three films, AFF observed a number of peaks, occurring at frequencies which they showed to be fit quite well by making a best guess for the thickness t of the film in question, and by assuming that peaks should occur at frequencies such that (according to the free-electron bulk-plasmon dispersion relation[4]) t equals an odd number of plasmon half-wavelengths. (MH's resonance condition.[1])

As is discussed in detail below,[5] because they restricted their attention at the outset to a film with identical surfaces, MH arrived at a criterion for the occurrence of resonant-bulk-plasmon-photoexcitation (RBPPE) peaks, which includes a special selection rule, viz., that no peaks should occur when t equals an *even* number of plasmon half-wavelengths. Since the AFF films did not have identical surfaces (the upper surface was a K-vacuum interface while the lower one was a K-silica substrate interface), it seems likely that AFF's use of the MH resonance condition led them to best-fit values of t which were on the order of twice too large.[5]

On the other hand, AFF's interpretation of their peaks as being a manifestation of RBPPE still seems correct, and so does the idea that RBPPE peak positions are fundamentally determined independently of a film's surface properties. The set of frequencies at which BPPE resonances can occur then, is *always* given by the film material's

bulk-plasmon dispersion relation and by the film thickness; the MH selection rule for a symmetric film shows, not how surface conditions can modify RBPPE peak positions, but rather how they can modulate RBPPE peak intensities[5] (or more generally, how they can affect RBPPE peak shapes).

The idea that film surface structure may be significant in determining RBPPE peak shapes is alluded to by AFF, who point out that among the possible reasons why their experimental peaks are broader than those calculated by MH are, not only MH's use of a bulk dielectric relaxation time which is unrealistically long ($\sim 50\omega_p^{-1}$ rather than $\sim 20\omega_p^{-1}$, where ω_p is the classical plasma frequency), but also their neglect of surface roughness and film-thickness nonuniformity. However, no quantitative work has been reported to date directed at explaining RBPPE peak shapes, nor in particular has there been any investigation of the intriguing possibility that they might contain useful surface-electronic-structure information.

Experimentally, at this time, there are several steps that would aid an investigation of the surface sensitivity of RBPPE phenomena. They are as follows:

(i) Since RBPPE peak positions for a symmetric film of thickness t are quite similar to those for an asymmetric film of thickness $\sim\frac{1}{2}t$, it would be useful, to resolve the ambiguity, to have RBPPE data from films of known (i.e., independently measured) thickness. Such data would thereby answer, also, the question of whether the seeming alternation of peak strengths seen in AFF's data is an indication of the near symmetry of their films and thus of the near satisfaction of MH's selection rule, or whether this behavior has some other cause.[5]

(ii) It would be useful to have RBPPE data as a function of film thickness, for fixed frequency. Such data would make it possible to sort out bulk-damping from surface-reflection effects in RBPPE peak shapes; this conclusion follows because bulk-damping effects should increase with film thickness while surface effects would remain the same.

(iii) It would be useful to have RBPPE data as a function of impurity adsorption. Changes in RBPPE peak shapes associated with adsorption would give an immediate experimental indication of how sensitive they are to surface conditions.

Theoretically, apart from surface irregularity effects (i.e., diffuse reflection) the influence of surface electronic structure on RBPPE peak shapes is shown, in Sec. II of this article, to be mediated by two complex, frequency-dependent parameters (per film surface): (i) p, which governs the probability that when a transverse electromagnetic wave strikes a surface (either from the vacuum or the metal side), a longitudinal wave will be generated, and (ii) s, which governs the probability that when a longitudinal wave strikes a surface, it will be reflected as a longitudinal wave rather than disappear with the simultaneous excitation of an electron-hole pair.

If $|p|$ and $|s|$ are large, then plasmons will be generated with relatively high probability when light strikes a surface, and they will not be severely damped upon reflection. Thus if $|p|$ and $|s|$ are large, plasmon resonances should be relatively strong and narrow; and vice versa.

At the outset then, in order to provide some idea of the theoretical surface sensitivity of RBPPE, Figs. 1(a) and 1(b) present plots of $|p|$ and $|s|$ vs ω for a variety of models of surface-electronic structure. The various models represented in the figures are as follows: (i) the model used by MH, viz., an electron gas whose density profile at a surface is a step function and whose dielectric response is hydrodynamic, and (ii) the models for which calculations are described below; in each case the behavior of the electromagnetic field is determined via a nonlocal conductivity tensor [calculated within the random phase approximation (RPA)] that corresponds to the choice of a model surface potential barrier $V(z)$. The potential barriers which are represented in Figs. 1(a) and 1(b) include the Lang-Kohn self-consistent potential[6] for r_s (the electron-gas radius) equal to 5 (approximately the value appropriate for potassium), and the potentials $V(z; w, \Phi)$ defined by

$$V(z; w, \Phi) = -\frac{\Phi + \mathcal{E}_F\,(r_s = 5)}{1 + \exp[-(z/w + z^3/125w^3)]}\ , \quad (1.1)$$

in which w and Φ represent the model surface diffuseness and work function, respectively. ($\mathcal{E}_F$ is the Fermi energy.)

Figures 1(a) and 1(b) reveal that $|p|$ and $|s|$ do depend appreciably on surface-electronic structure. The curves of Fig. 1(a) show their variation with potential barrier shape for Φ fixed (at its value, ~ 0.2 Ry,[6] for a clean K-vacuum interface), while Fig. 1(b) indicates their dependence on Φ for the barrier of Eq. (1.1) with $w = 0.5$ Å. The sensitivity of $|p|$ and of $|s|$ to Φ is particularly strong. Note, for example, that the plasmon reflectivity parameter $|s|$ increases rapidly to 1 as Φ increases from its clean-surface value through the photon energy $\hbar\omega$ (beyond which plasmon decay into a photoelectron-hole pair is impossible).

These results suggest that if one can extract experimental curves of $|p|$ and $|s|$ vs ω from data such as AFF's, one may indeed be able to use these curves to gain knowledge of surface-elec-

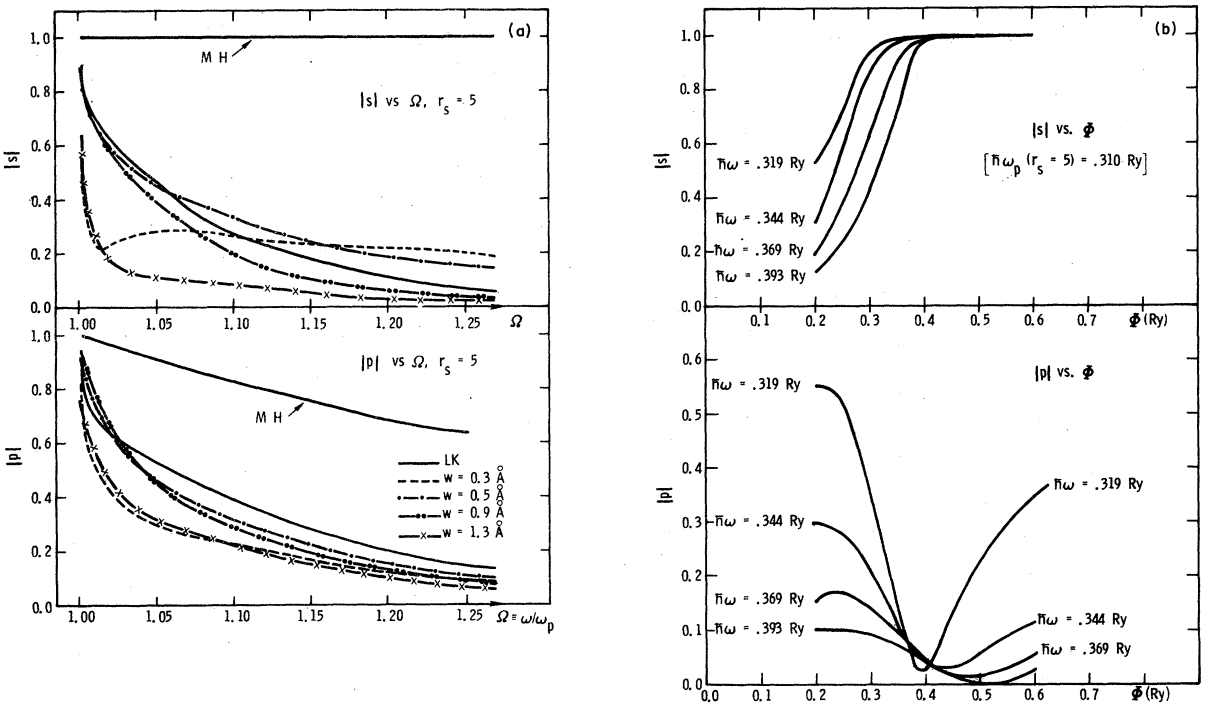

FIG. 1. (a) Frequency dependence of the parameters $|s|$ and $|p|$ which govern, respectively, the probability of plasmon reflection at a surface and the probability of transverse-to-longitudinal wave conversion there. Different curves correspond to different models of surface-electronic structure. That labeled MH corresponds to the hydrodynamic potassium surface model of Ref. 1. Solid curve (LK) corresponds to the use of the Lang-Kohn clean $r_s = 5$ jellium surface potential barrier (Ref. 6). Other curves (corresponding to various values of "w") were calculated using the potential barrier of Eq. (1.1) with the work function equal to approximately its clean potassium value (taken from Ref. 6), ~ 0.2 Ry. (b) Work-function dependence $|s|$ and $|p|$ for various frequencies ω. Calculations were performed using the potential barrier of Eq. (1.1) with $r_s = 5$ and w = 0.5 Å. Notice that both $|p|$ and $|s|$ undergo rapid variations as Φ increases through the value $\hbar\omega$ beyond which photoemission becomes impossible.

tronic structure; specifically, by determining what form of $V(z)$ provides the best description of the response of a free-electron metal surface to an incident electromagnetic wave.

Further calculated results for RBPPE-related experiments, which suggest that one is still some distance from achieving this goal, are presented in Sec. III. The reader who is mainly interested in assessing the present situation is therefore encouraged to skip over Sec. II, at a first reading. Section II contains a derivation of general microscopic formulas which describe the first-order (in the wave vector) corrections to the classical theory of the optical properties of a two-dimensionally translation-invariant solid. It also describes the use of these formulas to calculate RBPPE effects in optical reflection, transmission, and absorption as well as in photoemission.

II. MICROSCOPIC THEORY OF LONG-WAVELENGTH OPTICAL PROPERTIES OF THIN FREE-ELECTRON METAL FILM

In this section microscopic formulas are derived which enable one to compute lowest-order surface effects, particularly bulk-plasmon photoexcitation, in the optical properties of a thin, flat free-electron metal film, including not only its reflectivity and transmissivity, but also its photoelectric emissivity. The formulas are applicable for the case of long-wavelength light incident on the film.[7]

The basic assumption underlying the derivation is that, by virtue of the short healing distance in

the electron gas, film-thickness effects in the film's conductivity tensor can be ignored for thicknesses $\gtrsim 20$ Å. Thus in what follows the optical properties of a film are evaluated in terms of parameters characterizing a single surface. The remainder of this section is accordingly divided into two subsections, the first concerned with the scattering of electromagnetic waves at a single surface, and the second with the relation between the optical properties of a film and those of a semi-infinite metal.

A. Scattering of electromagnetic waves at surface of semi-infinite metal

Figure 2, schematically illustrates the rather complicated process which ensues when an electromagnetic wave of frequency $\omega > \omega_p$ is incident on a metal film. Both transverse and longitudinal waves are caused to propagate back and forth inside the film at the same time as the incident wave is reflected and transmitted back into the vacuum. The idea which enables one to analyze this process simply is to make use of the superposition principle which holds for sufficiently weak fields, and thus to represent the complicated process of Fig. 2 as a linear superposition of the processes illustrated in the five panels of Fig. 3. In what follows, then, I show how to solve Maxwell's wave equation in the long-wavelength limit for each of the relevant sets of boundary conditions: (a) a transverse wave incident from the vacuum onto a semi-infinite metal, (b) a transverse wave incident from the interior of a semi-infinite metal upon its surface, and (c) a longitudinal wave incident upon the surface of a semi-infinite metal from the interior. [Note that case (b) describes the situation illustrated in both Figs. 3(b) and 3(d) while case (c) describes those of Figs. 3(c) and 3(e). Thus only three types of boundary conditions are necessary to describe the five basic processes underlying that of Fig. 2.]

For an electromagnetic wave of frequency ω and wave vector $\vec{q}_\parallel$ along the flat surface of a semi-infinite jellium metal (which lies in the right half-space $z>0$), it is convenient to write the Maxwell wave equation in the form[8]

$$\vec{A}_{\vec{q}_\parallel\omega}(z) = \frac{4\pi}{q_\perp}\int_z^\infty dz' \sin q_\perp(z-z') \left\{ \frac{i\omega}{c^2}\int dz'' \vec{\vec{\sigma}}_{\vec{q}_\parallel\omega}(z',z'')\cdot\vec{A}_{\vec{q}_\parallel\omega}(z'') - \frac{1}{4\pi}\left(i\vec{q}_\parallel + \hat{u}_z\frac{\partial}{\partial z'}\right)\left[\left(i\vec{q}_\parallel + \hat{u}_z\frac{\partial}{\partial z'}\right)\cdot\vec{A}_{\vec{q}_\parallel\omega}(z')\right]\right\} , \tag{2.1}$$

wherein $\vec{A}_{\vec{q}_\parallel\omega}(z)$ is the electromagnetic vector potential (in the gauge for which the scalar potential vanishes identically), where $\vec{\vec{\sigma}}_{\vec{q}_\parallel\omega}(z',z'')$ is the sample's nonlocal conductivity tensor, where $\hat{u}_z$ is a unit vector pointing in the $+z$ direction (into the metal), and where $q_\perp \equiv [(\omega/c)^2 - |\vec{q}_\parallel|^2]^{1/2}$. Moreover, it is easy to verify that the asymptotic behavior of the most general solution to Eq. (2.1) is of the form[9]

$$\vec{A}_{\vec{q}_\parallel\omega}(z) = \vec{A}^0_{\vec{q}_\parallel\omega}\, e^{iq_\perp z} + \vec{R}_{\vec{q}_\parallel\omega}\, e^{-iq_\perp z}, \qquad z\to-\infty \tag{2.2a}$$

$$= \vec{T}^+_{\vec{q}_\parallel\omega}\, e^{iq_\perp^T z} + \vec{L}^+_{\vec{q}_\parallel\omega}\, e^{iq_\perp^L z} + \vec{T}^-_{\vec{q}_\parallel\omega}\, e^{-iq_\perp^T z} + \vec{L}^-_{\vec{q}_\parallel\omega}\, e^{-iq_\perp^L z}, \quad z\to+\infty, \tag{2.2b}$$

where $q_\perp^T$ is the z component of the classical transmitted-wave vector given by

$$q_\perp^{T2} \equiv q^{T2} - |\vec{q}_\parallel|^2 \tag{2.3a}$$

$$q^{T2}/\epsilon^T(q^T,\omega) = q^2 \equiv \omega^2/c^2 , \tag{2.3b}$$

[$\epsilon^T(q^T,\omega)$ is the metal's bulk, transverse dielectric constant], where $q_\perp^L$ is given by the solution to

$$\epsilon^L((q_\perp^{L2} + |\vec{q}_\parallel|^2)^{1/2},\omega) = 0 \tag{2.4}$$

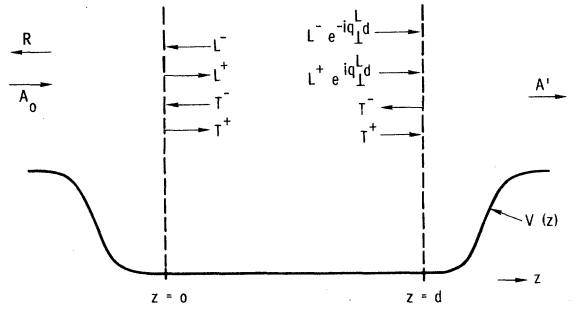

FIG. 2. Schematic indication of what happens when a transverse wave of amplitude A_0 impinges on a thin film. Transverse and longitudinal waves are excited in both directions ($\pm z$) in the film and reflected and transmitted waves are generated on either side of it. For a long-wavelength incident wave, the tranverse waves inside the film are also of long wavelength and therefore do not change phase or amplitude as they transverse the film.

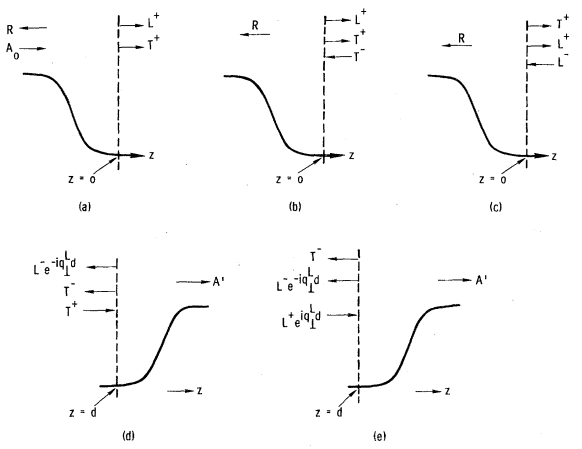

FIG. 3. Schematic drawings of the five elementary processes which combine linearly to constitute the transmission process of Fig. 2. (a) Transverse wave impinges on the $z=0$ surface from the vacuum creating "outgoing" transverse and longitudinal waves. (b) Reflected transverse wave impinges on the $z=0$ surface, with a similar result. (c) Reflected longitudinal wave strikes the $z=0$ surface with a similar result. (d) Transverse wave in the positive-z direction strikes the surface at $z=d$ generating reflected longitudinal and transverse waves as well as a wave transmitted into the vacuum. (e) Longitudinal wave on the positive-z direction strikes the $z=d$ surface with a similar result.

$$\vec{q}\cdot\vec{A}^{0}_{\vec{q}_\parallel\omega}=\vec{q}^{\,R}\cdot\vec{R}_{\vec{q}_\parallel\omega}=\vec{q}^{\,T^+}\cdot\vec{T}^{+}_{\vec{q}_\parallel\omega}=\vec{q}^{\,T^-}\cdot\vec{T}^{-}_{\vec{q}_\parallel\omega}=0\,, \tag{2.5}$$

$$\vec{q}^{\,L^+}\times\vec{L}^{+}_{\vec{q}_\parallel\omega}=\vec{q}^{\,L^-}\times\vec{L}^{-}_{\vec{q}_\parallel\omega}=0\,, \tag{2.6}$$

with

$$\vec{q}^{\,T^\pm}\equiv(\vec{q}_\parallel,\pm q_\perp^T),\quad \vec{q}^{\,L^\pm}\equiv(\vec{q}_\parallel,\pm q_\perp^L)\,,$$
$$\vec{q}\equiv(\vec{q}_\parallel,q_\perp),\quad \vec{q}^{\,R}\equiv(\vec{q}_\parallel,-q_\perp)\,. \tag{2.7}$$

The various sets of boundary conditions for which it is necessary to solve Eq. (2.1) can now be specified precisely. They are (a) $\vec{T}^{\pm}_{\vec{q}_\parallel\omega}=\vec{L}^{\pm}_{\vec{q}_\parallel\omega}=0$, (b) $\vec{A}^{0}_{\vec{q}_\parallel\omega}=\vec{L}^{\pm}_{\vec{q}_\parallel\omega}=0$, and (c) $\vec{A}^{0}_{\vec{q}_\parallel\omega}=\vec{T}^{\pm}_{\vec{q}_\parallel\omega}=0$.

In order to proceed, one specifies a value of z, called Z (which is typically of the order of a few angstroms), beyond which Eq. (2.2b) is true with negligible error. Then substituting Eq. (2.2b) into Eq. (2.1), the latter can be rewritten in a form which enables one to take explicit advantage of the fact that for light in the frequency range of interest ($\hbar\omega\lesssim 30$ eV), $|\vec{q}_\parallel|$, $q_\perp$ are small on the scale of typical microscopic inverse distances (such as the Fermi wave vector k_F and the inverse surface thickness). One thereby obtains the equation[9]

$$\vec{A}_{\vec{q}_\parallel\omega}(z)\approx\vec{A}^{\mathrm{I}}_{\vec{q}_\parallel\omega}(z;Z)+\vec{A}^{\mathrm{II}}_{\vec{q}_\parallel\omega}(z;Z)\,, \tag{2.8}$$

[$\epsilon^L(q^L,\omega)$ is the metal's bulk, longitudinal dielectric constant], and where $\vec{A}^{0}_{\vec{q}_\parallel\omega}$, $\vec{R}_{\vec{q}_\parallel\omega}$, $\vec{T}^{\pm}_{\vec{q}_\parallel\omega}$, and $\vec{L}^{\pm}_{\vec{q}_\parallel\omega}$ are constant vector amplitudes which satisfy

where $\vec{A}^{\mathrm{I}}$, the contribution to the right-hand side of Eq. (2.1) from the integration range $Z\lesssim z'<\infty$, is

$$\vec{A}^{\mathrm{I}}_{\vec{q}_\parallel\omega}(z;Z)=\left(\cos q_\perp(z-Z)+\frac{\sin q_\perp(z-Z)}{q_\perp}\frac{d}{dZ}\right)\left(\vec{T}^{+}_{\vec{q}_\parallel\omega}e^{iq_\perp^T Z}+\vec{T}^{-}_{\vec{q}_\parallel\omega}e^{-iq_\perp^T Z}+\frac{q^{L^2}}{q_\perp^{L^2}-q_\perp^2}\left(\vec{L}^{+}_{\vec{q}_\parallel\omega}e^{iq_\perp^L Z}+\vec{L}^{-}_{\vec{q}_\parallel\omega}e^{-iq_\perp^L Z}\right)\right), \tag{2.9}$$

and where $\vec{A}^{\mathrm{II}}$, the contribution from $z\lesssim z'\lesssim Z$ is

$$\vec{A}^{\mathrm{II}}_{\vec{q}_\parallel\omega}(z;Z)=\int_z^Z dz'\,\frac{\sin q_\perp(z-z')}{q_\perp}\left[q^2\vec{1}+\left(i\vec{q}_\parallel+\hat{u}_z\frac{d}{dz'}\right)\left(i\vec{q}_\parallel+\hat{u}_z\frac{d}{dz'}\right)\right]$$
$$\times\frac{4\pi i}{\omega}\int dz''\,\vec{\sigma}_{\vec{q}_\parallel\omega}(z',z'')\cdot\vec{A}_{\vec{q}_\parallel\omega}(z'')\,. \tag{2.10}$$

The expansion of Eq. (2.9) in powers of the small wave vectors $q_\perp$ and $q_\perp^T$ is straightforward. Assuming that $q_\perp z$, $q_\perp Z$, $q_\perp^T z$, and $q_\perp^T Z$ are all $\ll 1$, one obtains through first order the expression

$$\vec{A}^{\mathrm{I}}_{\vec{q}_\parallel\omega}(z;Z)\approx\vec{T}^{+}_{\vec{q}_\parallel\omega}(1+iq_\perp^T z)+\vec{T}^{-}_{\vec{q}_\parallel\omega}(1-iq_\perp^T z)+\left(1+(z-Z)\frac{d}{dZ}\right)\left(\vec{L}^{+}_{\vec{q}_\parallel\omega}e^{iq_\perp^L Z}+\vec{L}^{-}_{\vec{q}_\parallel\omega}e^{-iq_\perp^L Z}\right)+\cdots\,. \tag{2.11}$$

The expansion of Eq. (2.10) is somewhat more complicated. To begin, making use of the facts that $\sigma^{xy}_{\vec{q}_\parallel\to 0,\omega}(z,z')$, $\sigma^{zy}_{\vec{q}_\parallel\to 0,\omega}(z,z')$, and $\sigma^{zx}_{\vec{q}_\parallel\to 0,\omega}(z',z'')$ are, respectively, of $O(q_xq_y)$, $O(q_y)$, and $O(q_x)$,[10] one finds through first order that

$$\vec{A}^{\parallel}_{\vec{q}_\parallel\omega}(z;Z)=\frac{4\pi i}{\omega}\int_z^Z dz'(z-z')\frac{d}{dz'}\int dz''\left[i\vec{q}_\parallel\sigma^{zz}_{\vec{q}_\parallel\to 0,\omega}(z'z'')A^{z}_{\vec{q}_\parallel\omega}(z'')\right.$$
$$\left.+\hat{u}_z\left(\sigma^{xx}_{\vec{q}_\parallel\to 0,\omega}(z'z'')\,i\vec{q}_\parallel\cdot\vec{A}^{\parallel}_{\vec{q}_\parallel\omega}(z'')+\frac{d}{dz'}\sigma^{z\gamma}_{\vec{q}_\parallel\to 0,\omega}(z'z'')A^{\gamma}_{\vec{q}_\parallel\to 0,\omega}(z'')\right)\right], \tag{2.12}$$

where summation on the index $\gamma=x, y, z$ is implied.

Integrating by parts on z', and making use of the assumption that for z' in the neighborhood of Z, $\vec{\sigma}_{\vec{q}_\parallel\omega}(z', z'')$ has healed to its bulk (translation and rotation invariant) form,[11] Eq. (2.12) may be reduced to the expressions[12]

$$\vec{A}^{\parallel}_{\vec{q}_\parallel\omega}(z;Z)=-i\vec{q}_\parallel\int_z^Z dz'(z-z')\frac{dA_{\vec{q}_\parallel\omega}}{dz'} \tag{2.13}$$

and

$$\vec{A}^{\parallel}_{\vec{q}_\parallel\omega}{}^{z}(z;Z)=[\epsilon^T(0,\omega)-1]\,[T^{+z}_{\vec{q}_\parallel\omega}(1+iq_\perp^T Z)+T^{-z}_{\vec{q}_\parallel\omega}(1-iq_\perp^T Z)]-\left(1+(z-Z)\frac{d}{dZ}\right)(L^{+z}_{\vec{q}_\parallel\omega}e^{iq_\perp^L Z}+L^{-z}_{\vec{q}_\parallel\omega}e^{-iq_\perp^L z})$$
$$+\frac{4\pi i}{\omega}\int dz'\left(\int_z^Z dz''\,\sigma^{xx}_{0\omega}(z',z'')\,i\vec{q}_\parallel\cdot\vec{A}^{\parallel}_{\vec{q}_\parallel\omega}(z'')-\sigma^{z\gamma}_{\vec{q}_\parallel\to 0,\omega}(z,z')A^{\gamma}_{\vec{q}_\parallel\omega}(z')\right). \tag{2.14}$$

Substituting Eqs. (2.11), (2.13), and (2.14) into Eq. (2.8), and using the fact that[10] both

$$\int dz'\,\sigma^{zx}_{\vec{q}_\parallel\to 0,\omega}(z,z') \quad\text{and}\quad \int dz'\,\sigma^{zy}_{\vec{q}_\parallel\to 0,\omega}(z,z')$$

are at least of $O(q_\parallel^2)$, one obtains the greatly simplified[13] long-wavelength form of Eq. (2.1),

$$A^{z}_{\vec{q}_\parallel\omega}(z)=T^{+z}_{\vec{q}_\parallel\omega}[\epsilon^T(0,\omega)+iq_\perp^T z]+T^{-z}_{\vec{q}_\parallel\omega}[\epsilon^T(0,\omega)-iq_\perp^T z]$$
$$+\left([\epsilon^T(0,\omega)-1]\,iq_\perp^T Z(T^{+z}_{\vec{q}_\parallel\omega}-T^{-z}_{\vec{q}_\parallel\omega})+\frac{4\pi i}{\omega}\int_z^Z dz'\int dz''\,\sigma^{xx}_{0\omega}(z',z'')\,i\vec{q}_\parallel\cdot\vec{A}^{\parallel}_{\vec{q}_\parallel\omega}(z'')\right)$$
$$-\frac{4\pi i}{\omega}\int dz''\,\sigma^{zz}_{0\omega}(z,z'')A^{z}_{\vec{q}_\parallel\omega}(z'') \tag{2.15}$$

and

$$\vec{A}^{\parallel}_{\vec{q}_\parallel\omega}(z)\approx\vec{T}^{+\parallel}_{\vec{q}_\parallel\omega}(1+iq_\perp^T z)+\vec{T}^{-\parallel}_{\vec{q}_\parallel\omega}(1-iq_\perp^T z)+(\vec{q}_\parallel/q_\perp^T)(L^{+z}_{\vec{q}_\parallel\omega}e^{iq_\perp^L z}-L^{-z}_{\vec{q}_\parallel\omega}e^{-iq_\perp^L z})$$
$$-i\vec{q}_\parallel\int_z^Z dz'\,[A^{z}_{\vec{q}_\parallel\omega}(z')-L^{+z}_{\vec{q}_\parallel\omega}e^{iq_\perp^L z'}-L^{-z}_{\vec{q}_\parallel\omega}e^{-iq_\perp^L z'}-T^{+z}_{\vec{q}_\parallel\omega}-T^{-z}_{\vec{q}_\parallel\omega}]. \tag{2.16}$$

[Note that Z in Eq. (2.16) can now be set equal to ∞. As will be shown below, this limit can also be taken explicitly in Eq. (2.15). Thus this arbitrary cutoff parameter does not affect any of the results found for $\vec{A}_{\vec{q}_\parallel\omega}(z)$, as, of course, it should not.]

All of the results presented in this paper are based on the solution of Eqs. (2.15) and (2.16) using approximate forms of $\vec{\sigma}_{0\omega}(z', z'')$, and for various sets of boundary conditions. Before attempting to solve for $\vec{A}_{\vec{q}_\parallel\omega}(z)$, however, it is worth noting that from the very forms of Eqs. (2.15) and (2.16) one can deduce the microscopic generalizations of the classical matching conditions across a surface, which enable one to write formal expressions for the reflection and transmission amplitudes for electromagnetic waves impinging on it.

In order to derive matching conditions for $A^{z}_{\vec{q}_\parallel\omega}(z)$, first note that, according to Eq. (2.16), $\vec{A}^{\parallel}_{\vec{q}_\parallel\omega}(z)$ is independent of z to zeroth order in $\vec{q}_\parallel$. (This fact in itself represents the classical matching condition for the tangential electric field across the surface.) As a result, in Eq. (2.15), since one is only interested in retaining first order in $|\vec{q}_\parallel|$, the third term on its right-hand side can be replaced by the expression

$$\{[\epsilon^T(0,\omega)-1]iq_\perp^T Z(T^{+z}_{\vec{q}_\parallel\omega}-T^{-z}_{\vec{q}_\parallel\omega})$$
$$+i\vec{q}_\parallel\cdot(\vec{T}^{+\parallel}_{\vec{q}_\parallel\omega}+\vec{T}^{-\parallel}_{\vec{q}_\parallel\omega})f_\omega(z;Z)\}, \tag{2.17}$$

where the function $f_\omega(z;Z)$, defined by

$$f_\omega(z;Z)\equiv\frac{4\pi i}{\omega}\int_z^Z dz'\int dz''\,\sigma^{xx}_{0\omega}(z',z''), \tag{2.18}$$

has the useful asymptotic properties

$$f_\omega(z;Z)\to[\epsilon^T(0,\omega)-1](Z-z),\quad z\to\infty \tag{2.19a}$$

$$\to[\epsilon^T(0,\omega)-1](Z-a),\quad z\to-\infty, \tag{2.19b}$$

where a is a constant. Substitution of Eqs. (2.17) and (2.19) into Eq. (2.15) reveals the asymptotic behavior of $A^{\pm z}_{q_\parallel\omega}(z)$, viz.,[14]

$$A^{\pm z}_{q_\parallel\omega}(z)\to T^{\pm z}_{q_\parallel\omega}(1+iq_\perp^T z)+T^{\mp z}_{q_\parallel\omega}(1-iq_\perp^T z)+L^{\pm z}_{q_\parallel\omega}e^{iq_\perp^L z}+L^{\mp z}_{q_\parallel\omega}e^{-iq_\perp^L z},\quad z\to\text{“}\infty\text{”} \tag{2.20a}$$

$$\to T^{\pm z}_{q_\parallel\omega}[\epsilon^T(0,\omega)(1+iq_\perp^T a)+iq_\perp^T(z-a)]+T^{\mp z}_{q_\parallel\omega}[\epsilon^T(0,\omega)(1-iq_\perp^T a)-iq_\perp^T(z-a)],\quad z\to-\text{“}\infty\text{”}. \tag{2.20b}$$

The matching conditions for $A^{\pm z}_{q_\parallel\omega}(z)$ are derived from the comparison of Eqs. (2.20b) and (2.2a). In order to obtain familiar looking results one may either choose the origin of z such that the quantity a equals zero, or one can redefine $\vec{T}^{\pm}_{q_\parallel\omega}$, $\vec{R}^{\pm}_{q_\parallel\omega}$, and $\vec{A}^{0}_{q_\parallel\omega}$:

$$\vec{T}^{\pm}_{q_\parallel\omega}\to\vec{T}^{\pm}_{q_\parallel\omega}e^{\pm iq_\perp^T a},\quad \vec{R}^{\pm}_{q_\parallel\omega}\to\vec{R}^{\pm}_{q_\parallel\omega}e^{iq_\perp a},\quad \vec{A}^{0}_{q_\parallel\omega}\to\vec{A}^{0}_{q_\parallel\omega}e^{-iq_\perp a}. \tag{2.21}$$

Adopting this latter course, Eqs. (2.20) become

$$A^{\pm z}_{q_\parallel\omega}(z)\to T^{+z}[1+iq_\perp^T(z-a)]+T^{-z}[1-iq_\perp^T(z-a)]+L^{\pm z}_{q_\parallel\omega}e^{iq_\perp^L z}+L^{\mp z}_{q_\parallel\omega}e^{-iq_\perp^L z},\quad z\to\infty \tag{2.22a}$$

$$A^{\mp z}_{q_\parallel\omega}(z)\to T^{\pm z}_{q_\parallel\omega}[\epsilon^T(0,\omega)+iq_\perp^T(z-a)]+T^{\mp z}_{q_\parallel\omega}[\epsilon^T(0,\omega)-iq_\perp^T(z-a)],\quad z\to-\infty; \tag{2.22b}$$

Eq. (2.2a) undergoes a similar change. Thus the comparison of Eqs. (2.22b) and (2.2a) yields the matching conditions

$$A^{0z}_{q_\parallel\omega}+R^{z}_{q_\parallel\omega}=\epsilon^T(0,\omega)(T^{\pm z}_{q_\parallel\omega}+T^{\mp z}_{q_\parallel\omega})+O(|\vec{q}_\parallel|^2,q_\perp^2,q_\perp^{T\,2}) \tag{2.23}$$

and

$$q_\perp(A^{0z}_{q_\parallel\omega}-R^{z}_{q_\parallel\omega})=q_\perp^T(T^{\pm z}_{q_\parallel\omega}-T^{\mp z}_{q_\parallel\omega})+O(|\vec{q}_\parallel|^2,q_\perp^2,q_\perp^{T\,2}). \tag{2.24}$$

Equation (2.23) is, of course, the classical matching condition for the normal component of the displacement and is seen here to be valid through first order in the small wave vectors. For p-polarized light, incident in the x-y plane, one may rewrite Eq. (2.24) [using Eqs. (2.5)] in the form

$$A^{0x}_{q_\parallel\omega}+R^{x}_{q_\parallel\omega}=T^{\mp x}_{q_\parallel\omega}+O(q_\parallel,q_\perp,q_\perp^T), \tag{2.25}$$

which is the classical matching condition for the tangential component of the electric field. [For s-polarized light Eq. (2.24) is vacuous to lowest orders in $\vec{q}_\parallel,q_\perp,q_\perp^T$.] Note however that the corrections to Eq. (2.25) are of first order in the small wave vectors. Thus unlike Eq. (2.23), Eq. (2.25) is of no use in evaluating the lowest corrections to the classical description of the behavior of an electromagnetic field at a surface.

In order to obtain another *useful* matching condition, one returns to Eq. (2.16), which, incorporating the redefinition of $\vec{T}^{\pm}_{q_\parallel\omega}$ discussed above [Eq. (2.21)], implies the asymptotic behavior of $\vec{A}^{\parallel}_{q_\parallel\omega}(z)$[14]:

$$\vec{A}^{\parallel}_{q_\parallel\omega}(z\to\text{“}\infty\text{”})\to\vec{T}^{\pm\parallel}_{q_\parallel\omega}[1+iq_\perp^T(z-a)]+\vec{T}^{\mp\parallel}_{q_\parallel\omega}[1-iq_\perp^T(z-a)]+\vec{L}^{\pm\parallel}_{q_\parallel\omega}e^{iq_\perp^L z}+\vec{L}^{\mp\parallel}_{q_\parallel\omega}e^{-iq_\perp^L z} \tag{2.26a}$$

and

$$\vec{A}^{\parallel}_{q_\parallel\omega}(z\to-\text{“}\infty\text{”})\to\vec{T}^{\pm\parallel}_{q_\parallel\omega}+\vec{T}^{\mp\parallel}_{q_\parallel\omega}+ia\vec{q}_\parallel[\epsilon^T(0,\omega)-1](T^{\pm z}_{q_\parallel\omega}+T^{\mp z}_{q_\parallel\omega})-i\vec{q}_\parallel g_\omega(T^{\pm z}_{q_\parallel\omega}+T^{\mp z}_{q_\parallel\omega},L^{\pm z}_{q_\parallel\omega},L^{\mp z}_{q_\parallel\omega})+i(z-a)\{q_\perp^T(T^{\pm\parallel}_{q_\parallel\omega}-T^{\mp\parallel}_{q_\parallel\omega})+\vec{q}_\parallel[\epsilon^T(0,\omega)-1](T^{\pm z}_{q_\parallel\omega}+T^{\mp z}_{q_\parallel\omega})\}, \tag{2.26b}$$

where g_ω is defined by

$$g_\omega(T^{\pm z}_{q_\parallel\omega}+T^{\mp z}_{q_\parallel\omega},L^{\pm z}_{q_\parallel\omega},L^{\mp z}_{q_\parallel\omega})\equiv[\epsilon^T(0,\omega)-1](T^{\pm z}_{q_\parallel\omega}+T^{\mp z}_{q_\parallel\omega})Z-(L^{\pm z}_{q_\parallel\omega}e^{iq_\perp^L z}-L^{\mp z}_{q_\parallel\omega}e^{-iq_\perp^L z})/iq_\perp^L+\int_{-\infty}^{Z}dz'[A^z(z')-\epsilon^T(0,\omega)(T^{\pm z}_{q_\parallel\omega}+T^{\mp z}_{q_\parallel\omega})]. \tag{2.27}$$

Equation (2.26a) simply agrees with Eq. (2.2b), as it should. On the other hand, comparing Eq. (2.26b) and the modified version of Eq. (2.2a), one obtains a pair of matching conditions, namely,

$$\vec{A}^{0\parallel}_{\vec{q}_\parallel\omega}+\vec{R}^{\parallel}_{\vec{q}_\parallel\omega}=\vec{T}^{+\parallel}_{\vec{q}_\parallel\omega}+\vec{T}^{-\parallel}_{\vec{q}_\parallel\omega}+i\vec{a}\vec{q}_\parallel\,[\epsilon^T(0,\omega)-1]\times(T^{+z}_{\vec{q}_\parallel\omega}+T^{-z}_{\vec{q}_\parallel\omega})-i\vec{q}_\parallel g_\omega(T^{+z}_{\vec{q}_\parallel\omega}+T^{-z}_{\vec{q}_\parallel\omega},\,L^{+z}_{\vec{q}_\parallel\omega},\,L^{-z}_{\vec{q}_\parallel\omega})+O(|\vec{q}_\parallel|^2,q_\perp^{T2},q_\perp^2), \tag{2.28}$$

which is the generalization through first order in the small wave vectors of the classical boundary matching condition for the tangential electric field, and

$$q_\perp(\vec{A}^{0\parallel}_{\vec{q}_\parallel\omega}-\vec{R}^{\parallel}_{\vec{q}_\parallel\omega})=q_\perp^T(\vec{T}^{+\parallel}_{\vec{q}_\parallel\omega}-\vec{T}^{-\parallel}_{\vec{q}_\parallel\omega})+\vec{q}_\parallel[\epsilon^T(0,\omega)-1]\times(T^{+z}_{\vec{q}_\parallel\omega}+T^{-z}_{\vec{q}_\parallel\omega})+O(|\vec{q}_\parallel|^2,q_\perp^{T2},q_\perp^2), \tag{2.29}$$

which when rewritten in the form

$$(\vec{q}\times\vec{A}^0_{\vec{q}_\parallel\omega})_\parallel+(\vec{q}^R\times\vec{R}_{\vec{q}_\parallel\omega})_\parallel=(\vec{q}^{T+}\times\vec{T}^{+}_{\vec{q}_\parallel\omega})_\parallel+(\vec{q}^{T-}\times\vec{T}^{-}_{\vec{q}_\parallel\omega})_\parallel+O(|\vec{q}_\parallel|^2,q_\perp^{T2},q_\perp^2) \tag{2.30}$$

is recognized to be the classical matching condition for the tangential component of the magnetic field. [Note that, as with Eq. (2.25) above, Eq. (2.30) does not provide any information concerning first-order corrections to the classical result.]

For p-polarized light, the case of greatest interest,[15] Eqs. (2.15), (2.23), and (2.28) provide all the information necessary to calculate the lowest-order corrections to the reflection and transmission amplitude at a single surface. There are, as noted above, three cases of interest.

1. $\vec{T}_{\vec{q}_\parallel\omega}=\vec{L}^{-}_{\vec{q}_\parallel\omega}=0$

In this case one wishes to determine the reflection amplitude

$$M_{A^0,R}\equiv R^z_{\vec{q}_\parallel\omega}/A^{0z}_{\vec{q}_\parallel\omega}, \tag{2.31}$$

and the transmission amplitudes

$$M_{A^0,T^+}\equiv T^{+z}_{\vec{q}_\parallel\omega}/A^{0z}_{\vec{q}_\parallel\omega} \tag{2.32}$$

and

$$M_{A^0,L^+}\equiv L^{+z}_{\vec{q}_\parallel\omega}/A^{0z}_{\vec{q}_\parallel\omega}. \tag{2.33}$$

One begins by solving the appropriate zero-order (in the small wave vectors) version of Eq. (2.15), viz.,[16]

$$\mathfrak{A}_\omega(z)\equiv A^z_{\vec{q}_\parallel\omega}(z)/T^{+z}_{\vec{q}_\parallel\omega}=\epsilon^T(0,\omega)-\frac{4\pi i}{\omega}\int\sigma^{zz}_{0\omega}(z,z')\mathfrak{A}_\omega(z')\,dz'. \tag{2.34}$$

As $z\to-\infty$, one finds [cf., Eq. (2.2b)] that $\mathfrak{A}_\omega(z)$ is of the form

$$\mathfrak{A}_\omega(z\to-\infty)\to 1+pe^{iq_\perp^L z}. \tag{2.35}$$

Thus by virtue of the definition of $\mathfrak{A}_\omega(z)$ [Eq. (2.34)] one has that

$$p=L^{+z}_{\vec{q}_\parallel\omega}/T^{+z}_{\vec{q}_\parallel\omega}, \tag{2.36}$$

or in other words, that

$$M_{A^0,L^+}=pM_{A^0,T^+}. \tag{2.37}$$

In order to evaluate M_{A^0,T^+}, one now makes use of Eq. (2.36) and of the solution $\mathfrak{A}_\omega(z)$ to Eq. (2.34), to write

$$g_\omega(T^{+z}_{\vec{q}_\parallel\omega},L^{+z}_{\vec{q}_\parallel\omega},0)/T^{+z}_{\vec{q}_\parallel\omega}=g_\omega(1,p,0)=[\epsilon^T(0,\omega)-1]Z-pe^{iq_\perp^L Z}/iq_\perp^L+\int_{-\infty}^{Z}dz'[\mathfrak{A}_\omega(z')-\epsilon^T(0,\omega)]. \tag{2.38}$$

Combining Eqs. (2.5), (2.23), (2.28), and (2.38), one then obtains the expression

$$M_{A^0,T^+}=2\{\epsilon^T(0,\omega)+q_\perp^T/q_\perp+iq_\parallel^2/q_\perp[g_\omega(1,p,0)-[\epsilon^T(0,\omega)-1]a]\}^{-1}. \tag{2.39}$$

Finally, making use of Eq. (2.23) one obtains the expression for $M_{A^0,R}$:

$$M_{A^0,R}=\epsilon^T(0,\omega)M_{A^0,T^+}-1. \tag{2.40}$$

Thus all three amplitudes are determined in terms of the numerical solution of Eq. (2.34) for $\mathfrak{A}_\omega(z)$.

2. $\vec{A}^0_{\vec{q}_\parallel\omega}=\vec{L}^{-}_{\vec{q}_\parallel\omega}=0$

One begins again by solving the appropriate zero-order version of Eq. (2.15), which in this case is

$$\mathfrak{A}_\omega(z)\equiv A^z_{\vec{q}_\parallel\omega}(z)/(T^{+z}_{\vec{q}_\parallel\omega}+T^{-z}_{\vec{q}_\parallel\omega})=\epsilon^T(0,\omega)-\frac{4\pi i}{\omega}\int\sigma^{zz}_{0\omega}(z,z')\mathfrak{A}_\omega(z')\,dz'. \tag{2.41}$$

Note that this equation for $\mathfrak{A}_\omega(z)$ is identical to Eq. (2.34) except that now $\mathfrak{A}_\omega(z)$ is to be interpreted as $A^z_{\vec{q}_\parallel\omega}(z)/(T^{+z}_{\vec{q}_\parallel\omega}+T^{-z}_{\vec{q}_\parallel\omega})$. As a result,

the asymptotic behavior of $\mathfrak{A}_\omega(z)$ as $z \to \infty$ [Eq. (2.35)] now implies the relation

$$L^{+z}_{\vec{q}_\parallel \omega} = p(T^{+z}_{\vec{q}_\parallel \omega} + T^{-z}_{\vec{q}_\parallel \omega}), \tag{2.42}$$

or in other words, the relation

$$M_{T^-,L^+} = p(M_{T^-,T^+} + 1), \tag{2.43}$$

where

$$M_{T^-,L^+} \equiv L^{+z}_{\vec{q}_\parallel \omega} / T^{-z}_{\vec{q}_\parallel \omega} \tag{2.44}$$

and

$$M_{T^-,T^+} = T^{+z}_{\vec{q}_\parallel \omega} / T^{-z}_{\vec{q}_\parallel \omega}. \tag{2.45}$$

In order to determine the value of M_{T^-,T^+}, one makes use of Eq. (2.42) to write [cf., Eq. (2.27)]

$$g_\omega(T^{+z}_{\vec{q}_\parallel \omega} + T^{-z}_{\vec{q}_\parallel \omega}, L^{+z}_{\vec{q}_\parallel \omega}, 0) = (T^{+z}_{\vec{q}_\parallel \omega} + T^{-z}_{\vec{q}_\parallel \omega}) g_\omega(1, p, 0). \tag{2.46}$$

Combining Eqs. (2.5), (2.23), (2.28), and (2.38), one then obtains the expression

$$M_{T^-,T^+} = -\frac{(\epsilon^T(0,\omega) - q_\perp^T/q_\perp + (iq_\parallel^2/q_\perp)\{g_\omega(1,p,0) - [\epsilon^T(0,\omega) - 1]a\})}{(\epsilon^T(0,\omega) + q_\perp^T/q_\perp + (iq_\parallel^2/q_\perp)\{g_\omega(1,p,0) - [\epsilon^T(0,\omega) - 1]a\})}. \tag{2.47}$$

Finally, one makes use of Eqs. (2.23) to obtain the expression for the remaining amplitude M_{T^-R}, viz.,

$$M_{T^-R} \equiv R^z_{\vec{q}_\parallel \omega} / T^{-z}_{\vec{q}_\parallel \omega} = \epsilon^T(M_{T^-T^+} + 1), \tag{2.48}$$

which can be evaluated explicitly using Eq. (2.47).

3. $\vec{A}^0_{\vec{q}_\parallel \omega} = \vec{T}_{\vec{q}_\parallel \omega} = 0$

Again one begins by solving the appropriate zero-order version of Eq. (2.15); however, in this case it is essential to allow longitudinal waves traveling in both the plus- and minus-z directions in the asymptotic region $z \to \infty$. Thus, for example, one may set

$$\mathfrak{C}_\omega(z) \equiv A^z_{\vec{q}_\parallel \omega}(z) / L^{-z}_{\vec{q}_\parallel \omega} = \gamma \mathfrak{A}_\omega(z) + \mathfrak{B}_\omega(z), \tag{2.49}$$

where $\mathfrak{A}_\omega(z)$ and $\mathfrak{B}_\omega(z)$ satisfy the equations

$$\mathfrak{A}_\omega(z) = \epsilon^T(0,\omega) - \frac{4\pi i}{\omega} \int \sigma^{zz}(z,z') \mathfrak{A}_\omega(z')\, dz' \tag{2.50}$$

and

$$\mathfrak{B}_\omega(z) = -\frac{4\pi i}{\omega} \int \sigma^{zz}(z,z') \mathfrak{B}_\omega(z')\, dz', \tag{2.51}$$

respectively, subject to the boundary conditions

$$\mathfrak{A}_\omega(z \to \infty) \to 1 + pe^{iq_\perp^L z}, \tag{2.52}$$

$$\mathfrak{B}_\omega(z \to \infty) \to e^{-iq_\perp^L z} + se^{iq_\perp^L z}. \tag{2.53}$$

The constant γ in Eq. (2.49) is then determined by requiring $\mathfrak{C}_\omega(z)$ to satisfy the tangential boundary condition Eq. (2.28).

Even without determing the value of γ, one may make use of Eqs. (2.49), (2.52), and (2.53) to obtain consistency relations among the scattering amplitudes relevant to the present case. Specifically, combining these three relations, one has that

$$\mathfrak{C}_\omega(z \to \infty) \to \gamma + (\gamma p + s)e^{iq_\perp^L z} + e^{-iq_\perp^L z}, \tag{2.54}$$

which when compared to Eq. (2.2b) implies the formulas

$$M_{L^-T^+} \equiv T^{+z}_{\vec{q}_\parallel \omega} / L^{-z}_{\vec{q}_\parallel \omega} = \gamma \tag{2.55}$$

and

$$M_{L^-L^+} \equiv L^{+z}_{\vec{q}_\parallel \omega} / L^{-z}_{\vec{q}_\parallel \omega} = \gamma p + s. \tag{2.56}$$

Thus independent of the value of γ, one has the consistency relation

$$M_{L^-L^+} = pM_{L^-T^+} + s. \tag{2.57}$$

In addition, since $\vec{\sigma}_{\vec{q}_\parallel \omega}(z,z')$ vanishes rapidly as $z \to -\infty$ (i.e., as z is taken into the vacuum), the function $\mathfrak{B}_\omega(z)$ must also vanish rapidly in that limit. Therefore, one has that

$$\mathfrak{C}_\omega(z \to -\infty) \to \gamma \mathfrak{A}_\omega(z \to -\infty) \to \gamma \epsilon^T(0,\omega). \tag{2.58}$$

Comparing Eqs. (2.58) and (2.2a) one finds another consistency relation, i.e.,

$$M_{L^-R} \equiv R^z_{\vec{q}_\parallel \omega} / L^{-z}_{\vec{q}_\parallel \omega} = \gamma \epsilon^T(0,\omega) = \epsilon^T(0,\omega) M_{L^-T^+}. \tag{2.59}$$

Finally, in order to evaluate γ, one makes use of the relation [cf., Eq. (2.27)]

$$g_\omega(T^{+z}_{\vec{q}_\parallel \omega}, L^{+z}_{\vec{q}_\parallel \omega}, L^{-z}_{\vec{q}_\parallel \omega}) = [\gamma g^{\mathfrak{A}}_\omega(1,p,0) + g^{\mathfrak{B}}_\omega(0,s,1)] L^{-z}_{\vec{q}_\parallel \omega}, \tag{2.60}$$

where

$$g^{\mathfrak{A}}_\omega(1,p,0) = [\epsilon^T(0,\omega) - 1]Z - pe^{iq_\perp^L Z}/iq_\perp^L + \int_{-\infty}^{Z} dz' [\mathfrak{A}_\omega(z) - \epsilon^T(0,\omega)] \tag{2.61}$$

and

$$g^{\mathfrak{B}}_\omega(0,s,1) = -(se^{iq_\perp^L Z} - e^{iq_\perp^L Z})/iq_\perp^L + \int_{-\infty}^{Z} dz' \mathfrak{B}_\omega(z'). \tag{2.62}$$

Combining Eqs. (2.5), (2.28), (2.55), (2.57), and

(2.60) one obtains the formula

$$\gamma=(-iq_{\parallel}^2/q_{\perp})g_{\omega}(0,s,1)(\epsilon^T(0,\omega)+q_{\perp}^T/q_{\perp} +(iq_{\parallel}^2/q_{\perp})\{g_{\omega}^{\alpha}(1,p,0)-[\epsilon^T(0,\omega)-1]a\})^{-1}, \tag{2.63}$$

in terms of which explicit values of $M_{L^-L^+}$, $M_{L^-T^+}$, and M_{L^-R} can be calculated.

Thus the formal evaluation of the scattering matrix elements at a single surface is complete.

B. Optical properties of film in terms of those of single surface

In this section formulas for the optical properties of a film are derived in terms of the single-surface scattering amplitudes obtained in Sec. II A. The basic assumption underlying the derivation is that the film is sufficiently thick that the scattering at either surface is independent of that at the other. Thus the complicated process illustrated in Fig. 2 can be treated as a simple superposition of the five processes illustrated in Fig. 3, and, in particular, the amplitudes of the outgoing waves generated at $z=0$ in Fig. 2 satisfy equations

$$R_{\mathbf{q}_{\parallel}\omega}^{s}=M_{A^0R}A_{\mathbf{q}_{\parallel}\omega}^{0s}+M_{T^-R}T_{\mathbf{q}_{\parallel}\omega}^{-s}+M_{L^-R}L_{\mathbf{q}_{\parallel}\omega}^{-s}, \tag{2.64a}$$

$$T_{\mathbf{q}_{\parallel}\omega}^{\pm s}=M_{A^0T^+}A_{\mathbf{q}_{\parallel}\omega}^{0s}+M_{T^-T^+}T_{\mathbf{q}_{\parallel}\omega}^{-s}+M_{L^-T^+}L_{\mathbf{q}_{\parallel}\omega}^{-s}, \tag{2.64b}$$

$$L_{\mathbf{q}_{\parallel}\omega}^{\pm s}=M_{A^0L^+}A_{\mathbf{q}_{\parallel}\omega}^{0s}+M_{T^-L^+}T_{\mathbf{q}_{\parallel}\omega}^{-s}+M_{L^-L^+}L_{\mathbf{q}_{\parallel}\omega}^{-s}, \tag{2.64c}$$

while those for the waves generated at $z=d$ satisfy

$$A_{\mathbf{q}_{\parallel}\omega}^{\prime s}=\bar{M}_{T^+A'}T_{\mathbf{q}_{\parallel}\omega}^{\pm s}+\bar{M}_{L^+A'}L_{\mathbf{q}_{\parallel}\omega}^{\pm s}e^{iq_{\perp}^{L}d}, \tag{2.65a}$$

$$T_{\mathbf{q}_{\parallel}\omega}^{-s}=\bar{M}_{T^-T^+}T_{\mathbf{q}_{\parallel}\omega}^{\pm s}+\bar{M}_{L^+T^-}L_{\mathbf{q}_{\parallel}\omega}^{\pm s}e^{iq_{\perp}^{L}d}, \tag{2.65b}$$

$$L_{\mathbf{q}_{\parallel}\omega}^{-s}e^{-iq_{\perp}^{L}d}=\bar{M}_{T^+L^-}T_{\mathbf{q}_{\parallel}\omega}^{\pm s}+\bar{M}_{L^+L^-}L_{\mathbf{q}_{\parallel}\omega}^{\pm s}e^{iq_{\perp}^{L}d} \tag{2.65c}$$

(provided that d is not too large[17]). In Eq. (2.64), the matrix elements are those calculated in Sec. II A, while in Eq. (2.65), the matrix elements $\bar{M}$ are the analogous quantities calculated for the surface at $z=d$ (which, in general, will be different from the $z=0$ surface).

In order to obtain formulas for a film's optical properties, one simply needs to solve Eqs. (2.64) and (2.65) for $R_{\mathbf{q}_{\parallel}\omega}^{s}$, $A_{\mathbf{q}_{\parallel}\omega}^{\prime s}$, $T_{\mathbf{q}_{\parallel}\omega}^{\pm s}$, and $L_{\mathbf{q}_{\parallel}\omega}^{\pm s}$ in terms of $A_{\mathbf{q}_{\parallel}\omega}^{0s}$. The reflectivity and transmissivity of the film (for p-polarized light) can then be calculated via the equations

$$\mathcal{R}_{\mathbf{q}_{\parallel}\omega}^{(p)}=|R_{\mathbf{q}_{\parallel}\omega}^{s}/A_{\mathbf{q}_{\parallel}\omega}^{0s}|^2 \tag{2.66}$$

and (assuming that both interfaces are with the vacuum)

$$\mathcal{T}_{\mathbf{q}_{\parallel}\omega}^{(p)}=|A_{\mathbf{q}_{\parallel}\omega}^{Ls}/A_{\mathbf{q}_{\parallel}\omega}^{0s}|^2. \tag{2.67}$$

The explicit solution of Eqs. (2.64) and (2.65) is greatly simplified if one takes advantage of the consistency relations Eqs. (2.37), (2.43), and (2.57) satisfied by the M's and $\bar{M}$'s. In particular, using these relations to substitute for M_{A^0L}, $M_{T^-L^+}$, and $M_{L^-L^+}$ in Eq. (2.64c), and combining the resulting equation with Eq. (2.64b) one finds the relation

$$L_{\mathbf{q}_{\parallel}\omega}^{\pm s}-sL_{\mathbf{q}_{\parallel}\omega}^{-s}=pt_{\mathbf{q}_{\parallel}\omega}^{\pm}, \tag{2.68}$$

where the quantity $t_{\mathbf{q}_{\parallel}\omega}^{\pm}$ is defined by

$$t_{\mathbf{q}_{\parallel}\omega}^{\pm}\equiv T_{\mathbf{q}_{\parallel}\omega}^{\pm s}+T_{\mathbf{q}_{\parallel}\omega}^{-s}. \tag{2.69}$$

Operating similarly on Eqs. (2.65b) and (2.65c) one finds that

$$L_{\mathbf{q}_{\parallel}\omega}^{-s}e^{-iq_{\perp}^{L}d}-\bar{s}L_{\mathbf{q}_{\parallel}\omega}^{\pm s}e^{iq_{\perp}^{L}d}=\bar{p}t_{\mathbf{q}_{\parallel}\omega}^{\pm}, \tag{2.70}$$

where $\bar{p}$ and $\bar{s}$ are the amplitudes for the surface at $z=d$, which are analogous to p and s.

One may now combine Eqs. (2.68) and (2.70), leading to the useful relations

$$L_{\mathbf{q}_{\parallel}\omega}^{\pm s}/L_{\mathbf{q}_{\parallel}\omega}^{-s}=e^{-iq_{\perp}^{L}d}(p+\bar{p}se^{iq_{\perp}^{L}d})/(\bar{p}+p\bar{s}e^{iq_{\perp}^{L}d}) \tag{2.71}$$

and

$$L_{\mathbf{q}_{\parallel}\omega}^{-s}/t_{\mathbf{q}_{\parallel}\omega}^{\pm}=(\bar{p}+p\bar{s}e^{iq_{\perp}^{L}d})/(e^{-iq_{\perp}^{L}d}-s\bar{s}e^{iq_{\perp}^{L}d}). \tag{2.72}$$

Equations (2.71) and (2.72) combined with Eq. (2.65c) immediately yield an expression for $T_{\mathbf{q}_{\parallel}\omega}^{-s}/T_{\mathbf{q}_{\parallel}\omega}^{\pm s}$. This expression and Eq. (2.72) may then be substituted in Eq. (2.64b) yielding the solution for $T_{\mathbf{q}_{\parallel}\omega}^{\pm s}/A_{\mathbf{q}_{\parallel}\omega}^{0s}$ and ultimately leading to the complete solution of Eqs. (2.64) and (2.65).

In the case of a symmetric film (i.e., one with identical surfaces) for which the barred amplitudes are equal to the corresponding unbarred ones (i.e., $\bar{p}=p$, $\bar{s}=s$, $\bar{M}_{L^+L^-}=M_{L^-L^+}$, etc.), the final results are particularly simple. One finds, for this case, that

$$\mathcal{T}_{\mathbf{q}_{\parallel}\omega}^{(p)}=|1+F_{\mathbf{q}_{\parallel}\omega}^{(p)}|^{-2} \tag{2.73a}$$

and

$$\mathcal{R}_{\mathbf{q}_{\parallel}\omega}^{(p)}=|F_{\mathbf{q}_{\parallel}\omega}^{(p)}/(1+F_{\mathbf{q}_{\parallel}\omega}^{(p)})|^2, \tag{2.73b}$$

where

$$F_{\mathbf{q}_{\parallel}\omega}^{(p)}\equiv[iq_{\parallel}^2/q_{\perp}\epsilon^T(0,\omega)]\{g_{\omega}^{\alpha}(1,p,0) -[\epsilon^T(0,\omega)-1]a+[p/(e^{-iq_{\perp}^{L}d}-s)]g_{\omega}^{\alpha}(0,s,1)\}. \tag{2.74}$$

For the classical model treated by Melnyk and Harrison,[1] namely a film with identical geometrically sharp surfaces at $z=0$ and $z=d$, and with a dielectric behavior given entirely by the bulk dielectric constants $\epsilon^T(q^T,\omega)$ and $\epsilon^L(q^L,\omega)$, it can easily be shown (see Appendix) that the equations

$$g_{\omega}^{\alpha}(1,p,0)=[1-\epsilon^T(0,\omega)]/iq_{\perp}^{L},$$
$$g_{\omega}^{\alpha}(0,s,1)=2/iq_{\perp}^{L}, \tag{2.75}$$
$$s=-1,\quad p=\epsilon^T(0,\omega)-1,\quad a=0$$

are satisfied. Substituting Eqs. (2.75) into Eq.

(2.74) one thus obtains the expression

$$F^{\mathrm{MH}}_{\vec{q}_\parallel\omega} = \left(\frac{1}{\epsilon^T(0,\omega)} - 1\right)\frac{q_\parallel^2}{i q_\perp q_\perp^L}\tan\tfrac{1}{2}q_\perp^L d, \qquad (2.76)$$

which agrees, as it should, with the MH result [cf. Eqs. (2.52a) and (2.52b) of Ref. 1]. Thus the microscopic equations presented here yield the correct classical limit.

The final topic to be treated in this section is the photoemissivity of a metal film. For photon frequencies in the range $1 < \omega/\omega_p \lesssim 1.5$, one can calculate the photoemission probability to lowest order via a simple model, because at these energies the photoelectron mean free path λ is typically $\gtrsim 15$ Å, a value large compared to the surface thickness but small compared to typical film thicknesses d. Thus to lowest order one may assume (i) that only electrons emitted directly into the vacuum (i.e., which do not transverse the film) are detected, but (ii) that λ can be neglected in calculating the probability of photoexcitation at either of the film surfaces.

With these two assumptions the photocurrent emitted per incident photon, from that surface of a film upon which the photons are incident, is given by the formula[18]

$$\frac{d^2Y_\omega}{d\Omega_f\, dE_f} = \frac{S}{\cos\theta_I}\frac{|t^+_{\vec{q}_\parallel\omega}|^2}{|\vec{A}^0_{\vec{q}_\parallel\omega}|^2}\, Q_\omega(\Omega_f, E_f), \qquad (2.77)$$

where S is the film surface area, θ_I is the angle of incidence of the photon beam, $\Omega_f \equiv (\theta_f, \varphi_f)$, and E_f are the emergence angle and energy of the photoelectrons, where t^+ is defined in Eq. (2.69), and where

$$\begin{aligned} Q_\omega(\Omega_f, E_f) \equiv{}& (\alpha/\pi^2\hbar\omega)\Theta(\hbar\omega - \Phi - E_f^{(\perp)}) \\ &\times\Theta(E_f^{(\perp)} + \Phi + \mathcal{E}_f - \hbar\omega) \\ &\times[E_f/(E_f^{(\perp)} + \Phi + \mathcal{E}_f - \hbar\omega)]^{1/2} \\ &\times(|\mathfrak{M}_{fi}|^2 + |\mathfrak{M}^{(c)}_{fi}|^2)_{E_i^{(\perp)} = E_f^{(\perp)} - \hbar\omega}. \end{aligned} \qquad (2.78)$$

In Eq. (2.78), Φ is the film's work function, $\mathcal{E}_F$ is its Fermi energy, α is the fine-structure constant, $E_f^{(\perp)}$ and $E_i^{(\perp)}$ are the initial and final electron energies due to motion normal to the surface, and the matrix elements $\mathfrak{M}_{fi}$ and $\mathfrak{M}^{(c)}_{fi}$ are defined by

$$\mathfrak{M}_{fi} = \int dz\, j_{fi}(z) A^z_{\vec{q}_\parallel\omega}(z)/t^+_{\vec{q}_\parallel\omega} \qquad (2.79a)$$

and

$$\mathfrak{M}^{(c)}_{fi} = \int dz\, j^*_{fi}(z) A^z_{\vec{q}_\parallel\omega}(z)/t^+_{\vec{q}_\parallel\omega}, \qquad (2.79b)$$

where

$$j_{fi}(z) \equiv \psi_f^* \frac{d\psi_i}{dz} - \psi_i^*(z)\frac{d\psi_f}{dz}, \qquad (2.80)$$

$\psi_i(z)$ and $\psi_f(z)$ being the initial and final photoelectron wave functions, respectively.

In order to evaluate $\mathfrak{M}_{fi}$ and $\mathfrak{M}^{(c)}_{fi}$, one solves the Schrödinger equation

$$\left(-\frac{\hbar^2}{2m}\frac{d^2}{dz^2} + V(z) - E_{f,i}^{(\perp)}\right)\psi_{f,i}(z) = 0 \qquad (2.81)$$

for the photoelectron wave functions,[19] and one takes $A^z_{\vec{q}_\parallel\omega}/t^+_{\vec{q}_\parallel\omega}$ from the equation

$$\frac{A^z_{\vec{q}_\parallel\omega}}{t^+_{\vec{q}_\parallel\omega}} = \mathfrak{A}_\omega(z) + \frac{\bar{p} + p\bar{s}e^{iq_\perp^L d}}{e^{-iq_\perp^L d} - s\bar{s}e^{iq_\perp^L d}}\,\mathfrak{B}_\omega(z), \qquad (2.82)$$

which, as may be easily verified, satisfies Eqs. (2.64) and (2.65) in addition to solving Eq. (2.15). [$\mathfrak{A}_\omega(z)$ and $\mathfrak{B}_\omega(z)$ are defined in Eqs. (2.50)–(2.53).] The photoemission results presented in Sec. III are all based on the numerical evaluation of Eq. (2.77) via Eqs. (2.78)–(2.82).

III. NUMERICAL RESULTS AND DISCUSSION

This section is devoted to a numerical study of RBPPE phenomena in photoemission from free-electron metal films, and particularly to the question of their sensitivity to surface electronic structure. The study necessarily begins with the specification of a "reasonable" approximate form of the nonlocal conductivity tensor $\vec{\sigma}_{\vec{q}_\parallel\to 0,\,\omega}(z, z')$ to substitute into the (exact) formulas of Sec. II. Two criteria guide the choice of an approximate $\vec{\sigma}_{\vec{q}_\parallel\to 0,\,\omega}(z, z')$: (i) The approximation must be sufficiently general as to accommodate a variety of surface models. (Thus, e.g., an approximation which presupposes surfaces at which electrons are confined by a square-step potential barrier would be too restrictive.) (ii) The approximation should give a correct account of the film material's bulk optical properties, e.g., the calculated reflectivity for a thick film should agree with experiment.[20] Unfortunately there does not appear to exist any simple approximation to $\vec{\sigma}_{\vec{q}_\parallel\to 0,\,\omega}(z, z')$ which satisfies both these criteria simultaneously. Thus in what follows, a form of $\vec{\sigma}_{\vec{q}_\parallel\to 0,\,\omega}(z, z')$ is chosen, which sacrifices the exact satisfaction of the second criterion, but thereby preserves the generality required by the first.

To begin, let us consider adopting the RPA form of $\vec{\sigma}_{\vec{q}_\parallel\to 0,\,\omega}(z, z')$,[9]

$$\begin{aligned} \sigma^{\gamma,\gamma'}_{\vec{q}_\parallel\to 0,\,\omega}(z, z') = -\frac{e^2}{i\omega}\,\delta_{\gamma\gamma'}\Bigg(&\frac{n_0(z)}{m}\delta(z - z') \\ &+ \frac{2}{\hbar}\int\frac{d^2k}{\pi^2}\int_{K,K'}\frac{\theta_{kK} - \theta_{kK'}}{\omega + i\delta - \omega_{K'} + \omega_K} \\ &\times j^\gamma_{kK'}(z) j^{\gamma'}_{k'K}(z')\Bigg). \end{aligned} \qquad (3.1)$$

In Eq. (3.1) the current density $j^\gamma_{kK'}(z)$ is defined

$$j^{\gamma}_{K,K'}(z)=\frac{\hbar}{2mi}\left(\psi^{*}_{K}(z)\frac{d\psi_{K'}}{dz}-\frac{d\psi^{*}_{K}(z)}{dz}\psi_{K'}(z)\right),\quad \gamma=3\equiv z$$
$$=\frac{\hbar k^{\gamma}}{m}\psi^{*}_{K}(z)\psi_{K'}(z),\quad \gamma=1,2\equiv x,y\,, \tag{3.2}$$

where the $\psi_K(z)$ are the single-electron wave functions of the free-electron metal in its ground state, thus the $\psi_K(z)$ [as well as the ω_K of Eq. (3.1)] are obtained via the Schrödinger equation

$$\left(-\frac{\hbar^2}{2m}\frac{d^2}{dz^2}+V(z)-\hbar\omega_K\right)\psi_K(z)=0\,, \tag{3.3}$$

where $V(z)$ is a single-electron potential barrier which represents the electronic structure of the unperturbed metal's surfaces.

The K and K' integrals of Eq. (3.1) cover all solutions to Eq. (3.3) above as well as below the vacuum level, and the quantities $\theta_{k,K}$ are the zero-temperature Fermi function, i.e.,

$$\theta_{k,K}\equiv\theta\left(\mathcal{E}_F-\frac{\hbar^2k^2}{2m}-\hbar\omega_K\right), \tag{3.4}$$

where

$$\mathcal{E}_F\equiv\hbar^2k_F^2/2m \tag{3.5}$$

is the Fermi energy and $\theta(x)$ is the ordinary step function. Finally, $n_0(z)$ is the unperturbed metal's electron density profile; that is,[9]

$$n_0(z)=2\int\frac{d^2k}{(2\pi)^2}\int_0^{\infty}\frac{2\,dK}{\pi}\theta_{k,K}|\psi_K(z)|^2\,. \tag{3.6}$$

It should be noted in passing that the choice of the specific approximate form, Eq. (3.1), for $\sigma^{\gamma\gamma'}_{\vec{q}_{\parallel}\to 0,\omega}(z,z')$ automatically implies the choice for a form for the transverse dielectric constant $\epsilon^T(0,\omega)$, which, cf., Eqs. (2.34), (2.41), and (2.50), is required in solving for the electromagnetic field in the surface region. In particular, Eq. (3.1) implies[9] the relation

$$\epsilon^T(0,\omega)=1-\omega_p^2/\omega^2\,. \tag{3.7}$$

The RPA form of $\sigma^{\gamma\gamma'}_{\vec{q}_{\parallel}\to 0,\omega}(z,z')$ specified in Eq. (3.1) has a number of virtues. Specifically, (i) it can be expected to yield a reasonable qualitative description of the collective response of an electron gas to an imposed electromagnetic field (see, however, the limitation noted below); and (ii) permits the study of the sensitivity to surface electronic structure of a film's optical properties insofar as Eq. (3.1) imposes no *a priori* restriction on the spatial form of the surface potential barrier $V(z)$ [Eq. (3.3)], which ultimately determines the specific form of $\sigma^{\gamma\gamma'}_{\vec{q}_{\parallel}\to 0,\omega}(z,z')$.

Moreover (and significantly), computer methods for evaluating the RPA conductivity tensor and using it to solve for electromagnetic fields near surfaces have previously been developed and tested.[9]

On the other hand, the use of Eq. (3.1) has a number of important disadvantages; in particular, the RPA conductivity of that equation cannot yield an accurate quantitative description of the optical properties (including the photoelectric yield[21]) of any real metal because (a) it does not incorporate *any* bulk damping [i.e., the effective relaxation time in Eq. (3.1), and consequently in Eq. (3.7), is infinite]; and (b) it includes neither dynamical exchange[22a] nor interband effects[22b] on bulk plasmon dispersion, even though both are believed to be quantitatively significant.[22]

Additionally, since the use of Eq. (3.1) yields values of the plasmon reflection amplitude s which are generally rather small [cf., Fig. 1(a) for Φ equal to the clean potassium work function ($\sim$0.2 Ry), and for all the forms of $V(z)$ that were tested, $|s|$ was found to be $<30\%$ for $\Omega>1.1$], it thereby leads to the prediction of RBPPE features in photoemission which seem decidedly too broad when compared to the AFF data. This discrepancy can be remedied somewhat (see, e.g., Fig. 11) by increasing the values of Φ used for one or both of the film surfaces; which [cf. Fig. 1(b)] leads to sharply increased values of $|s|$; and indeed one can even justify the use of higher than the clean surface values of Φ in terms of the facts that in the AFF experiment the lower film surface was an interface with a silicon substrate, while the upper one may not have been perfectly clean. However, it may be that at least part of the discrepancy is due to a more fundamental problem than the use of poor forms of $V(z)$ to describe the AFF surfaces, i.e., it may be due to the neglect in Eq. (3.1) of dynamical exchange and correlation effects or to the neglect of lattice periodicity.

These possibilities must clearly be studied eventually. However, for this first investigation of the surface sensitivity of RBPPE phenomena the advantages of using Eq. (3.1) clearly outweigh the disadvantages, and in what follows the results obtained within the RPA are presented and then compare to AFF's observations.

To begin, it is necessary to discuss the exact significance of AFF's data. In Fig. 4, reproduced from AFF's letter,[2] curves which are said to represent the wavelength derivative of photoyield versus photon energy are shown for potassium films (grown on silica substrates) whose thicknesses, according to AFF's best fit, were $\sim$27, $\sim$58, and $\sim$100Å. The following comments must be made regarding these curves:

(i) Although AFF state that the curves shown represent photoyields "measured relative to (that of) a reference film thicker than 500Å," it is perhaps not clear that what they mean[23] is that these curves

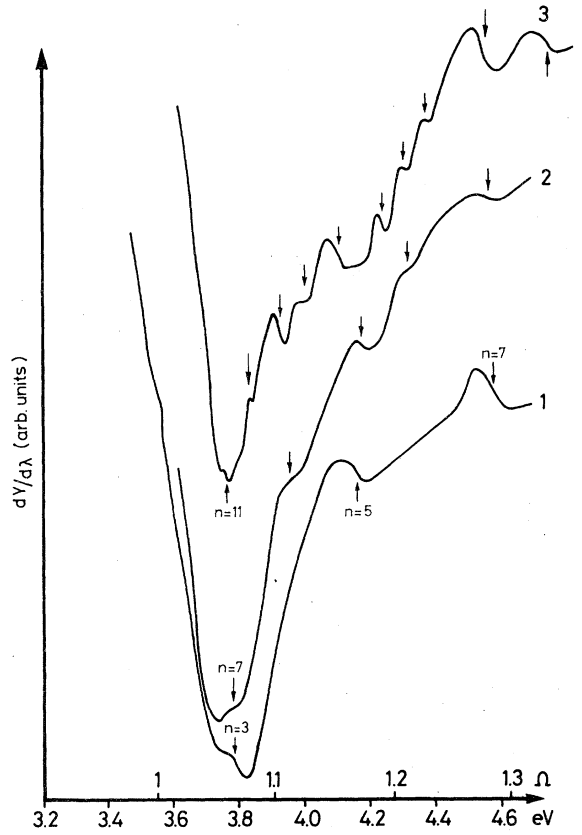

FIG. 4. Photoyield data of Anderegg *et al.* (reproduced, with permission, from Ref. 2). Curves are labeled 1, 2, and 3, and are found in Ref. 2 to represent potassium films of best-fit thicknesses 27, 58, and 100 Å, respectively. There is, however, reason to believe that their best-fit thicknesses may be about twice too large (Ref. 5). Labeling of the ordinate $dY/d\lambda$ in the figure is also probably in error; it should be presumably $-dY/d\lambda$ or perhaps $dY/d\omega$ (see text). Note that there is some indication of an alternation of peak strengths in all three curves; a possible explanation of this phenomenon is given in the text.

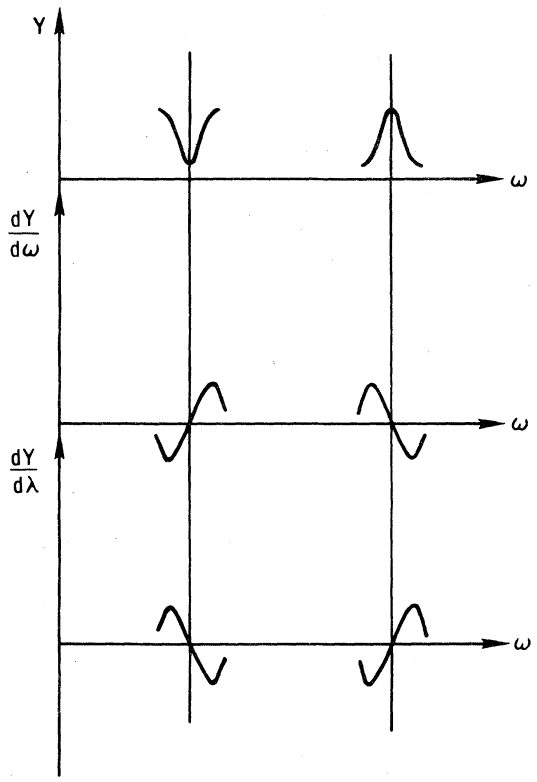

FIG. 5. Illustration of the reasoning leading to the conclusion that the ordinate of Fig. 4 is mislabeled. If a resonance structure in $Y(\omega)$ is a peak, then $dY/d\omega$ increases before it decreases. At the same time $dY/d\lambda$ decreases first. Since the resonance features in Fig. 4 clearly increase before they decrease and assuming that they correspond to resonant enhancement of Y (i.e., to a peak) they cannot be features in $dY/d\lambda$ but must represent either $-dY/d\lambda$ or $dY/d\omega$.

represent not simply the photoyields measured from their three thin films, but rather that each curve represents the photoyield from one of the thin films *minus* the photoyield from a reference film of thickness >500Å.

(ii) Although the ordinate in Fig. 4 is labeled $dY/d\lambda$, it is hard to believe that the curves shown do not actually represent $-dY/d\lambda$ or $dY/d\omega$. The point is, as is illustrated in Fig. 5, that if the labeling of the ordinate of Fig. 4 is correct, then the resonance structures observed by AFF were in fact *dips* in the photoyield γ and not peaks as AFF state (and as theory predicts). In what follows, therefore, it is assumed that the ordinate of Fig. 4 (AFF's Fig. 1) is mislabeled. (One of AFF has confirmed that this assumption is probably correct.[23]) With these remarks in mind, one now wishes to compute, for comparison with the AFF data, theoretical results for the *frequency* derivative of photoyields from thin films "relative to" (i.e., minus) that from a thick one. In what follows, just such results are presented. They have been obtained, by the straightforward application of the equations of Sec. II, using methods to solve for the relevant electromagnetic fields which have been described at length elsewhere.[9]

To begin, consider the photoyield curves of Figs. 6, which were calculated using the RPA conductivity tensor, with three different choices of the surface potential barrier $V(z)$ [specifically, the $r_s=5$ Lang-Kohn potential, and the hyperbolic tangent barriers of Eq. (1.1) with $w=0.5$ and 1.3 Å] for 58-Å thin films with identical clean surfaces. The results are calculated "relative to" those for

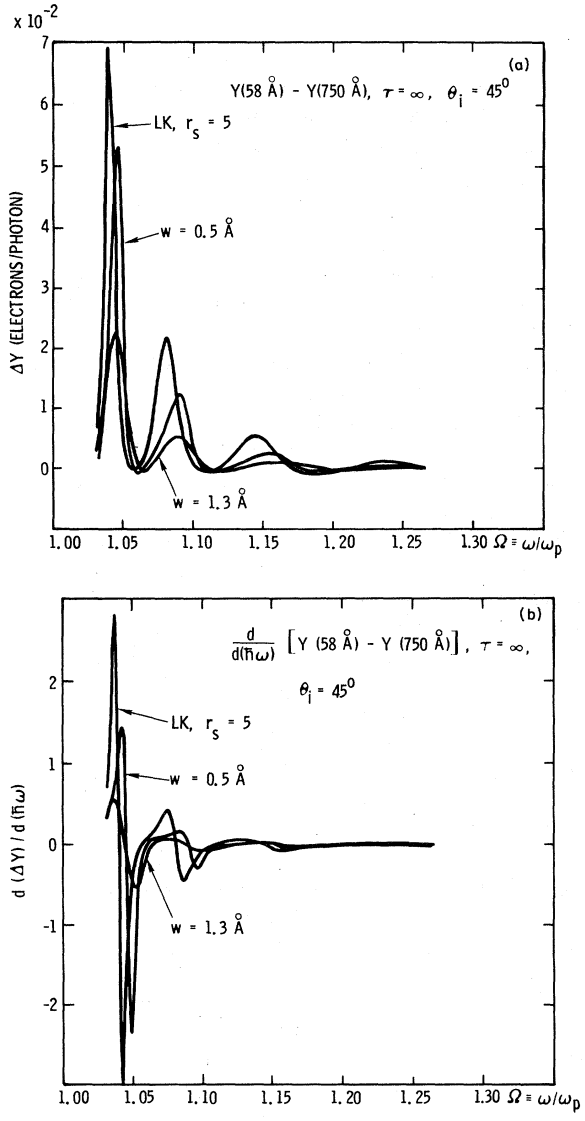

FIG. 6. (a) Photoyield calculated for a 58-Å, $r_s = 5$ jellium film minus that for a 750-Å film having the same surface structure. Calculations were carried out assuming a 45° angle of photon incidence θ_i and no bulk damping (i.e., relaxation time τ equal to ∞). Three curves correspond, respectively, to using the Lang-Kohn $r_s = 5$ surface potential barrier (Ref. 6), and to the barriers of Eq. (1.1) with $r_s = 5$, $\Phi \approx 0.2$ Ry, $w = 0.5$ Å and $w = 1.3$ Å. In each case the same potential barrier was used at both film surfaces. (b) Photon energy derivatives of the curves of Fig. 6(a). Note that these curves bear little resemblance to curve 2 of Fig. 4.

750-Å films.[24]

In passing, it should be noted that the distance a [cf. Eq. (2.19b)], which is used in evaluating the M's and $\bar{M}$'s of Eqs. (2.64) and (2.65), can be obtained straightforwardly from Eq. (3.1), which implies the formula

$$a = \lim_{z \to \text{“}\infty\text{”}} \left(Z - \int_{-\infty}^{z} dz\, n_0(z)/n_0(\text{“}\infty\text{”}) \right). \tag{3.8}$$

The thicknesses t of the films for which computed results are shown in Figs. 6 were assumed to be related to the parameter d (Fig. 2) by the equation

$$t = d + 2a, \tag{3.9}$$

which incorporates the thickness of a film's surface regions into the definition of its over-all thickness. This remark applies not only to Figs. 6, but to all the calculated results in this section.

All the curves of Figs. 6 clearly show resonance features due to BPPE. However it is evident that none of the curves of Fig. 6(b) bears much resemblance to the "58-Å" curve of Fig. 4. The main reason for this discrepancy is that within the RPA there is no bulk damping, and thus the use of Eq. (3.1) for $\sigma^{\gamma\gamma'}_{q_{\|}\omega}(z, z')$ gives a very poor account of the optical properties of a real metal film. (A film's photoelectric emissivity and its ordinary optical properties, e.g., its absorptivity, are obviously very closely related.[25])

In order to remedy the RPA's defective description of a real film's optical properties, one is immediately tempted to try incorporating damping effects via a "relaxation-time" approximation in which ω in Eq. (3.1) is replaced by $\omega + i/\tau(\omega)$, and consequently,[9] in which the bulk, transverse dielectric function is of the Drude form

$$\epsilon^T_\tau(\omega) = 1 - (\omega_p^2/\omega)/[\omega + i/\tau(\omega)]. \tag{3.10}$$

Through the use of Eq. (3.10), $\tau(\omega)$ can easily be fit to optical data for real metals. Unfortunately, however, while the replacement of ω by $\omega + i/\tau(\omega)$ in Eq. (3.1) does permit an improved description of the propagation of transverse waves in a metal, it also yields a description of longitudinal wave propagation which violates charge conservation.[26] A relatively simple prescription by which the relaxation time approximation can be made charge conserving has been given in Ref. 26. However, the simplicity of the method used there for a bulk metal does not carry over to the case of a sample having surfaces. Thus at least for the present no calculation has been undertaken in which Eq. (3.1) is modified to include relaxation effects while charge conservation is preserved. Instead use has been made of a somewhat *ad hoc* calculational recipe which is described in what follows.

The basis of the recipe is the fact that for free-electron metals, and for $\omega \sim \omega_p$, the bulk damping, though nonnegligible, is weak. That is, the inequality

$$\omega\tau(\omega)>>1 \tag{3.11}$$

is reasonably well satisfied. [For example, in Al, $\tau(\omega\approx\omega_p)\approx 30/\omega_p$,[27] while for K, $\tau(\omega\approx\omega_p)\approx 20/\omega_p$.[28]] The significance of Eq. (3.11) is that if it holds (and, cf. Fig. 7, if ω is not too close to ω_p), the changes in $A^z_{q_\parallel\omega}(z)$ caused by the fact that $\tau(\omega)\neq\infty$ can be expected to be important only on a scale of distances which is large compared to the thickness of a film surface. Thus the main effect of τ will be to cause a decrease in the amplitude of a longitudinal electromagnetic wave[29] as it traverses the interior of a film; otherwise there should be only slight modification due to τ in the spatial behavior of $A^z_{q_\parallel\omega}(z)$ in the surface region. This reasoning makes plausible the validity of the following calculational scheme: Wherever it appears in the formulas for the photoyield from a thin film [e.g., in Eqs. (2.65) and (2.82)], the quantity

$$\exp(iq_\perp^L d), \tag{3.12}$$

which represents the change in a plasmon's amplitude as it moves from $z=0$ to $z=d$, is replaced by the quantity

$$\exp[iq_\perp^L(\tau)d], \tag{3.13}$$

where, for example, the (complex) plasmon wave vector $q_\perp^L(\tau)$ is obtained from the charge-conserving bulk longitudinal dielectric function $\epsilon_\tau^L(q^L(\tau),\omega)$ of Ref. 26 by solving the equation

$$\epsilon_\tau^L(q_\perp^L(\tau),\omega)=0. \tag{3.14}$$

In addition, in order to account for the effect of $\tau(\omega)$ on transverse wave propagation in a film's interior, the Drude transverse dielectric function $\epsilon_\tau^T(\omega)$ [Eq. (3.10)] is used to calculate the M's and $\bar{M}$'s which appear in Eqs. (2.64) and (2.65). No other modifications are made in the formulas of Sec. II; in particular, the forms of the functions $\mathfrak{A}_\omega(z)$ and $\mathfrak{B}_\omega(z)$ which enter the calculation of the photoyield are taken to be unmodified by τ in the surface region.

Although this calculational prescription is not a fully consistent one—e.g., it neglects the bulk photoemission which must occur if $\tau(\omega)$ is finite—it does lead to results which, as can be seen in Figs. 8 and 9, resemble the AFF data far more closely than do the $\tau(\omega)=\infty$ results of Figs. 6. Thus it has been adopted for the present as a means for comparing RBPPE theory and experiment, and for discussing the surface sensitivity of RBPPE phenomena.

Although the curves of Figs. 8(b) and 9 certainly resemble the corresponding curves of Fig. 4 more closely than do any of the curves of Fig. 6(b), the results of Figs. 8(b) and 9 are still unsatisfactory in the following respects: (i) The large dip, which is present in all three curves of Fig. 4 is absent in the curves of Figs. 8(b) and 9; (ii) the number and positions of the RBPPE features in the curves of Figs. 8(b) and 9 disagree with the corresponding experimental results of Fig. 4; and, finally, (iii) the resonance structures in Figs. 8(b) and 9 are far broader than those of AFF's data—indeed, the peak widths in Figs. 8(b) and 9, in all the curves shown, are quite comparable to the peak separations, whereas the peaks in all three curves of Fig. 4 are well separated.

The explanation for the first discrepancy, the absence of the large dip in Figs. 8(b) and 9 at $\Omega\sim 1.07$, is simply that with the prescription which has been used to include the effects of bulk damping it is not possible to make reliable calculations too close to ω_p. This fact can be understood by reference to Fig. 7 in which values are shown of the complex plasmon wave vector $q_\perp^L(\tau)$ vs ω for $\tau=\infty$, $\tau=40/\omega_p$, and for the experimental $\tau(\omega)$ corresponding to potassium.[30] Note that for frequencies between ω_p and $1.05\omega_p$ the effect of even a "weak" bulk damping is large; the plasmon damping length is ~8 Å for τ equal to the experi-

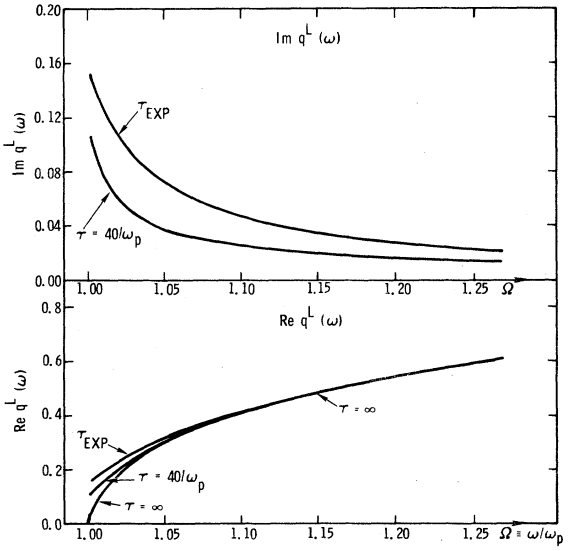

FIG. 7. Real and imaginary parts of the plasmon wave-vector q^L as a function of frequency calculated for $r_s=5$, and (1) no bulk damping ($\tau=\infty$), (2) damping given by the relaxation time $\tau=40/\omega_p$ ($r_s=5$), (3) damping given by a relaxation time $\tau(\omega)$ which rises from about $20/\omega_p$ at $\Omega=1$ to about $25/\omega_p$ at $\Omega=1.25$, in proportion to the rise indicated in the potassium optical data of Ref. 28. [Note that for $\tau=\infty$, $\mathrm{Im}q^L(\omega)\equiv 0$ in the frequency range shown.] Note that the effect of weak bulk damping on $q^L(\omega)$ is weak except when Ω is close to 1.

mental $\tau(\omega)$ in this frequency range.

If one were able to calculate reliably all the way down to ω_p, one would expect yield curves such as those of Fig. 8(a) to turn over and approach finite

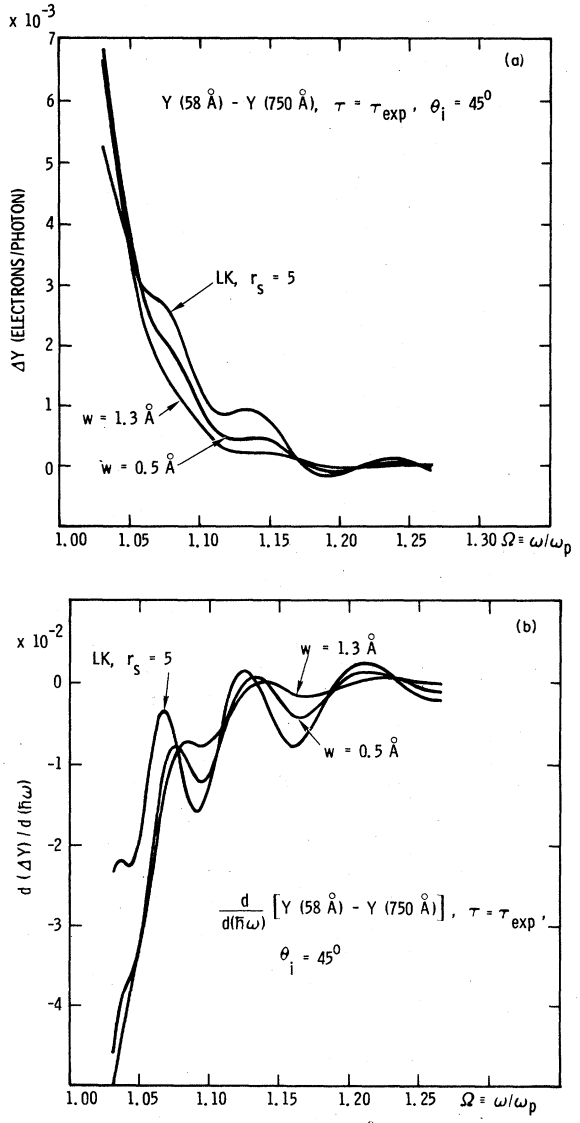

FIG. 8. (a) Photoyield from a 58-Å, $r_s = 5$ film minus that from a 750-Å film with the same surface structure. Photons are assumed to be incident at 45° and bulk damping effects were incorporated by the prescription given in the text, using a relaxation time $\tau(\omega)$ which increases from $\sim 20/\omega_p$ ($r_s = 5$) in proportion to the experimental $\tau(\omega)$ (Ref. 28). Three curves correspond, respectively, to the Lang-Kohn, $r_s = 5$, surface potential barrier (Ref. 6), and to the barriers of Eq. (1.1) with $r_s = 5$, $\Phi = 0.2$ Ry, and $w = 0.5$ Å and $w = 1.3$ Å. In each case the same potential was used at both film surfaces. (b) Photon energy derivatives of the curves of Fig. 8(a). Note that these curves resemble the data of Fig. 4 (curve 2) much more closely than do the curves of Fig. 6(b).

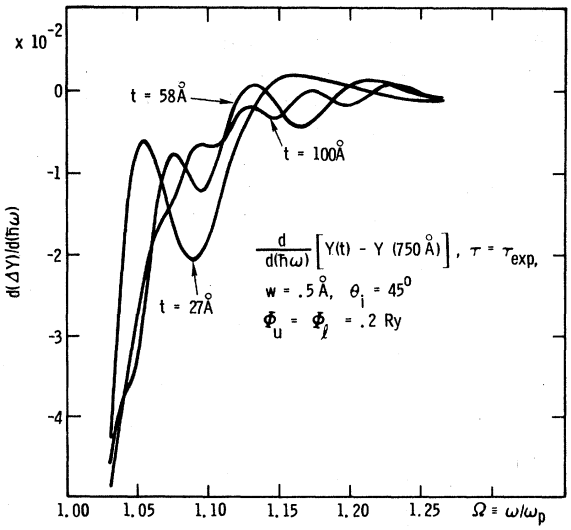

FIG. 9. Photon energy derivatives of photoyields from films of 27, 58, and 100 Å minus that from a 750-Å film. All these curves correspond to the use of the potential barrier of Eq. (1.1) with $w = 0.5$ Å, and the work functions at the upper and lower surfaces Φ_u and Φ_ℓ equal to 0.2 Ry. [Labels $\theta_i = 45°$ and $\tau = \tau_{exp}$ are explained in the caption of Fig. 8(a).]

values at ω_p; which would imply the existence of large dips in the corresponding derivative curves [e.g., those of Figs. 8(b) and 9] at approximately the correct positions.

The second discrepancy between the curves of Figs. 8(b) and 9 and the corresponding data of Fig. 4, namely, the disagreement in the number and positions of the RBPPE features, the following has twofold explanation:

(i) Equation (3.1) neglects dynamical exchange and correlation[22a] as well as interband[22b] effects; therefore the bulk plasmon dispersion relation which it implies [via Eq. (3.14)], and which determines the relative positions of RBPPE features in Figs. 8 and 9 (inasmuch as it determines the frequency dependence of the plasmon wave vector), is expected to be quantitatively inaccurate.[22a,b] And consequently, although the number of RBPPE features (say between $\Omega = 1$ and $\Omega = 1.3$) on any of the curves of Figs. 8 and 9 can be adjusted to agree with the data of Fig. 4 by changing the assumed values of the film thicknesses (one has the freedom to make such changes since AFF did not measure their film thicknesses absolutely), such changes will not remedy the discrepancy between the *positions* of the calculated and measured resonance features.

(ii) The calculations which underlie the curves of Figs. 8 and 9 were carried out for films having identical surfaces. However, this condition was

not satisfied in AFF's experiments; their films were grown on silica substrates and had nominally clean upper surfaces.

The remarkable effect of film asymmetry (i.e., of having inequivalent film surfaces) is illustrated in Figs. 10 and 11, in each of which photoyield versus frequency curves are shown corresponding to films with a fixed value of the work function at

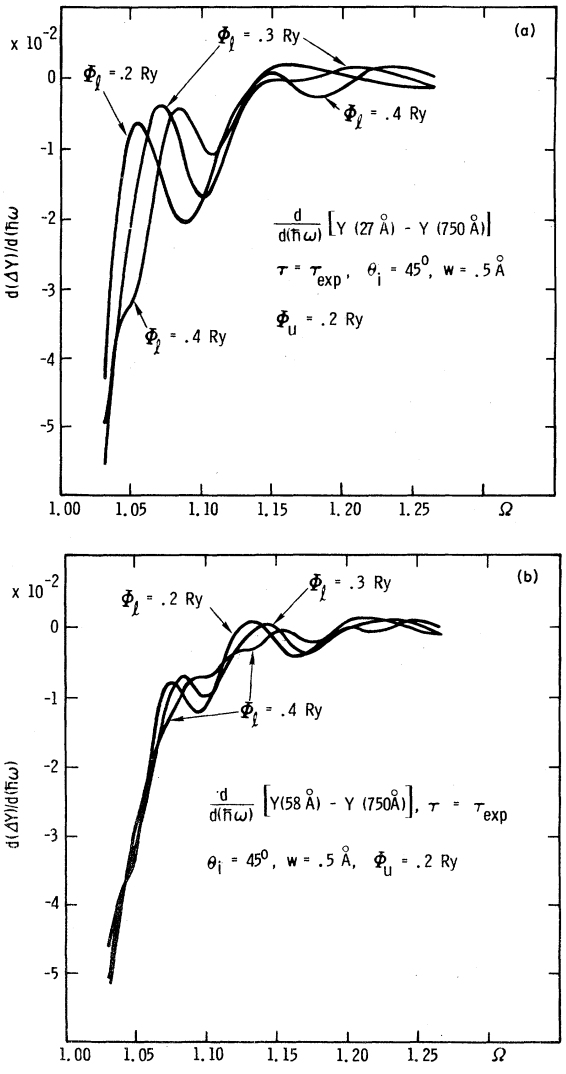

FIG. 10. (a) Illustration for a 27-Å film of the effects of having inequivalent surfaces. Photoyield derivative curves were calculated using the $V(z)$ of Eq. (1.1) with $w = 0.5$ Å for both upper and lower surfaces. But while Φ_u, the work function at the upper surface, was taken to equal 0.2 Ry in all three cases, Φ_l, the work function for the lower surface was taken to be 0.2, 0.3, and 0.4 Ry in the three different curves. [See Fig. 8(a) for the explanation of the labels $\theta_i = 45°$ and $\tau = \tau_{exp}$.] (b) Same as Fig. 10(a), for a 58-Å film.

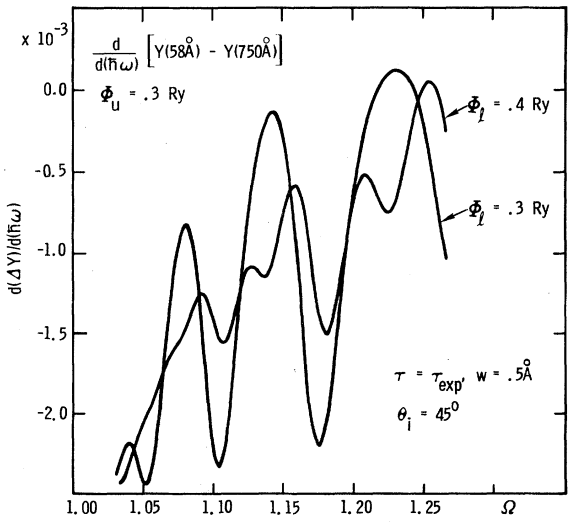

FIG. 11. Same as Fig. 10b, but for films with $\Phi_u = 0.3$ Ry and $\Phi_l = 0.3$ and 0.4 Ry at the lower surface.

the upper surface Φ_u and various values of that at the lower surface Φ_l. [All the calculations of Figs. 10 and 11 were done using the form of $V(z)$ given in Eq. (1.1) with $w = 0.5$Å at both upper and lower surfaces.] Note that as a film becomes asymmetric, one new RBPPE feature appears between each pair of features that were present for the asymmetric film of the same thickness.

The fact that for an asymmetric film one should see twice as many RBPPE features (per frequency interval) as for a symmetric film of the same thickness can be understood via Eqs. (2.77)–(2.79), and (2.82). These equations show that BPPE resonances arise in the theory from the rapid variation of the quantity [cf., Eq. (2.72)]

$$L^{z\bar{z}}_{q_{||}\omega}/t^{\pm}_{q_{||}\omega} = (\bar{p}e^{iq_\perp^L d} + p\bar{s}e^{2iq_\perp^L d})/(1 - s\bar{s}e^{2iq_\perp^L d}), \quad (3.15)$$

which represents the relative amplitudes of longitudinal and transverse waves excited in a thin film as an electromagnetic wave is transmitted through it. Since the denominator of Eq. (3.15), which represents the coherent addition of the amplitudes of plasmons reflected back and forth across the film, has a minimum whenever the quantity $s\bar{s}\exp(2iq_\perp^L d)$ is real and positive, Eq. (3.15) would lead us to expect the position of the nth BPPE resonance to be

$$(q_\perp^L)_n = n\pi/d - \arg(s\bar{s})/2d, \quad n = 0, 1, 2, \ldots . \quad (3.16)$$

However at the same time, according to Eq. (3.15), the variation of $L^{z\bar{z}}_{q_{||}\omega}/t^{\pm}_{q_{||}\omega}$ is also affected by the factor $\bar{p}\exp(iq_\perp^L d) + p\bar{s}\exp(2iq_\perp^L d)$, whose presence accounts for the additional interference effects which result from the fact that plasma waves

are coherently generated at the upper and lower film surfaces. In the general case, i.e., for an asymmetric film, the numerator factor will simply modulate the strengths of the RBPPE features seen. However for a symmetric film (i.e., one for which $p=\bar{p}$ and $s=\bar{s}$) the numerator cancels a factor in the denominator of Eq. (3.15). Thus the "modulation" of RBPPE peak strengths in the case of a symmetric film is quite drastic; it results, as can be seen in Figs. 10 and 11, in the annihilation of half the peaks which would otherwise be anticipated. [Mathematically the point is that if $\bar{p}=p$ and $\bar{s}=s$, then Eq. (3.15) reduces to

$$L^{-z}_{\vec{q}_{\parallel}\omega}/t^{+}_{\vec{q}_{\parallel}\omega}|_{\mathrm{sym}}=p/(e^{-iq_{\perp}^{L}d}-s). \tag{3.17}$$

BPPE resonances in this case will occur when the quantity $s\exp(iq_{\perp}^{L}d)$ is real and positive, and thus the nth resonance now occurs when the equation

$$(q_{\perp}^{L})_{n}=n\pi/d-\arg(-s)/d, \quad n=1,3,5,\ldots \tag{3.18}$$

is satisfied. Note that half the resonances are absent.]

Returning now to the comparison of theory with AFF's data, one notes that (a) if one wishes to fit AFF's data using a model which accounts for the asymmetry of their films, one is forced, by the fact that one sees twice as many RBPPE features in the asymmetric case as in the symmetric one, to assume film thicknesses of the order of *one-half* the AFF best-fit values. (b) However by doing so one may not only improve the agreement of theoretical and experimental resonance positions, but one may also be able to provide a simple explanation for what seems to be a fairly systematic alternation of peak strengths in AFF's curves (Fig. 4), namely, that the weak peaks are the ones that would disappear if the films were symmetric. [The weakness of these peaks can then be interpreted as a sign that the asymmetry of the electronic structure of AFF's films is relatively weak (cf., the results shown in Fig. 11).]

I return now to the third discrepancy, between the curves of Figs. 8 and 9 and those of Fig. 4, namely that the theoretical RBPPE features are too broad. This disagreement is directly traceable to the smallness, for the barriers used (which had $\Phi_u=\Phi_l=0.2\mathrm{Ry}\approx$ the value for clean potassium), of the parameter s which governs the plasmon reflectivity at the film surfaces. Thus in order to remedy it, the first possibility to check is that by using an increased work function at the lower surface—to represent in some degree the presence of AFF's silica substrate—one might find sharper theoretical RBPPE features. [Increasing Φ_l should sharpen these features because, cf. Fig. 1(b), $\bar{s}$ increases rapidly with increasing Φ_l.]

This effect is seen in Figs. 10, and might be made even more pronounced by an increase in Φ_u to account for the fact that the AFF surfaces may have been somewhat contaminated (cf. Fig. 11). However, in comparing the curves of Figs. 10 and 11 to the AFF data (recalling that because of film asymmetry effect one should compare the curves of Fig. 10(a) to AFF's "58-Å" curve and those of Figs. 10(b) and 11 to AFF's "100-Å" curve), it still seems as if the theoretical RBPPE features are somewhat too broad. The source of this disagreement is as yet unknown. It may be due to the fact that the forms tried for $V(z)$ are not sufficiently accurate (to predict large enough values of s and $\bar{s}$), or it may be due to the neglect of dynamical exchange and correlation or of lattice effects in the description of surface dielectric response provided by Eq. (3.1).

In any event it should now be clear what directions should be taken in both theoretical and experimental work concerning RBPPE phenomena. Theoretically, it is essential to replace Eq. (3.1) with a model conductivity tensor that yields *at least* a better description of a film material's bulk optical properties. Thus one must learn how to incorporate bulk damping effects consistently (presumably by generalizing the method of Ref. 26 for including a relaxation time without violating charge concentration); and one must develop a method for incorporating both dynamical exchange and correlation effects as well as those of lattice periodicity.

Experimentally, one must attempt to obtain RBPPE data from well-characterized samples. In particular, in order to permit a detailed analysis of the peak shapes, one would like to know the thicknesses of the films studied (via an independent, absolute measurement) as well as the conditions (smoothness, atomic composition) of both surfaces. (Obviously in order to know the condition of the lower surface of a film, the most favorable situation would be to have the film unsupported. The fact that such a situation is desirable however does not make it realizable.) It would also be useful to have data concerning the effects of altering surface conditions; for example, (a) a study of the effects on RBPPE of impurity adsorption (as noted in the Introduction) would give an immediate indication of the surface sensitivity of the data; (b) a study of the behavior of RBPPE features as a function of film asymmetry would be useful in confirming the predictions made above, i.e., the doubling of the number of RBPPE features as a film becomes asymmetric and an alternation in RBPPE peak strengths for a weakly asymmetric film.

The possible significance of carrying out this work is suggested by the results presented in Figs.

1 and 8, above. These figures indicate the inherent surface electronic structure dependence of RBPPE data.

APPENDIX

In this appendix Eqs. (2.75) are derived for the surface model used by MH (Ref. 1). The MH model assumes that the surface of a metal can be represented as a geometrically sharp plane (say at $z=0$). To the left of the plane there is vacuum (and thus the conductivity tensor is zero), while to the right is metal whose dielectric response is that of an infinite metal. Thus at the outset, the quantity a [cf. Eq. (2.19b)] is equal to zero by construction.

The quantities $g(1,p,0)$ and $g(0,s,1)$ can easily be calculated in the MH model by making use of the classical boundary condition

$$A^z + R^z = \epsilon^T (T^{+z} + T^{-z}), \tag{A1}$$

which, of course, the model must (and does) incorporate.

According to Eq. (A1) [in case 1, Sec. II A 1 ($T^{-z} \equiv 0$)], one has in the MH model

$$\begin{aligned} \mathfrak{A}_\omega(z) \equiv A^z(z)/T^{+z} &= \epsilon^T, \quad z<0 \\ &= 1 + p e^{iq_\perp^L z}, \quad z>0. \end{aligned} \tag{A2}$$

Substituting Eq. (A2) into Eq. (2.61) one thus finds the formula

$$g_\omega(1,p,0) = -p/iq_\perp^L. \tag{A3}$$

Similarly in the MH model one has [cf., Eq. (2.53)] that

$$\begin{aligned} \mathfrak{A}_\omega(z) &= 0, \quad z<0 \\ &= e^{-iq_\perp^L z} + s e^{iq_\perp^L z}, \quad z>0. \end{aligned} \tag{A4}$$

Substituting Eq. (A4) into Eq. (2.62) one finds the expression

$$g(0,s,1) = (1-s)/iq_\perp^L. \tag{A5}$$

Finally one needs expressions for p and s. These follow directly from MH's dynamical boundary condition, namely, the vanishing of the current normal to a surface at the surface. Assuming the surface to be at $z=0$ this condition may be expressed as

$$\sigma^T(0,\omega)(T^{z^+} + T^{z^-}) + \sigma^L(q_\perp^L,\omega)(L^{z^+} + L^{z^-}) = 0. \tag{A6}$$

In order to determine p one applies the conditions $L^{z^-} = T^{z^-} = 0$ of case 1 [Sec. II A 1. These conditions together with Eqs. (A6) and (2.4) imply that

$$p \equiv L^{z^+}/T^{z^+} = \epsilon^T(0,\omega) - 1. \tag{A7}$$

Finally to determine s, one imposes (in the $\vec{q}_\parallel \to 0$ limit) the conditions of case 3 (Sec. II A 3), viz., $T^{+z} = 0$ and $T^{-z} \approx 0$. These conditions together with Eq. (A6) yield the formula

$$s \equiv L^{+z}/L^{-z} = -1. \tag{A8}$$

Substituting Eqs. (A7) and (A8), respectively, into Eqs. (A3) and (A5), one then has derived all of Eqs. (2.75).

---

*Work supported by the U. S. Energy Research and Development Administration.

[1] A. R. Melnyk and M. J. Harrison, Phys. Rev. B 2, 835 (1970); see also, R. Fuchs and K. L. Kliewer, Phys. Rev. 185, 905 (1969); and W. E. Jones, K. L. Kliewer, and R. Fuchs, *ibid.* 178, 1201 (1969).

[2] M. Anderegg, B. Feuerbacher, and B. Fitton, Phys. Rev. Lett. 27, 1565 (1971); see also, I. Lindau and P. O. Nilsson, Phys. Lett. 31, A352 (1970); Phys. Scr. 3, 87 (1971).

[3] Although only optical measurements were discussed in Ref. 1, as is pointed out by AFF, photoyield should be approximately proportional to optical absorption for thin films.

[4] See, e.g., D. Pines and P. Nozières, *Theory of Quantum Liquids* (Benjamin, New York, 1966).

[5] In addition to the discussion given in this article, see P. J. Feibelman, Phys. Rev. Lett. 35, 617 (1975).

[6] N. D. Lang and W. Kohn, Phys. Rev. B 1, 4555 (1970).

[7] That is, the wavelength (or attenuation distance) of the transverse wave inside the film is also assumed to be long (on the scale of the film thickness).

[8] See, P. J. Feibelman [Phys. Rev. B 12, 1319 (1975)] for the derivation of Eq. (2.1).

[9] See, P. J. Feibelman, Phys. Rev. B 12, 1319 (1975).

[10] By rotational invariance in the x-y plane, P. J. Feibelman (unpublished).

[11] P. M. Platzman and P. A. Wolff, *Solid State Physics*, edited by F. Seitz and D. Turnbull (Academic, New York, 1973), Suppl. No. 13.

[12] The derivation of Eq. (2.13) makes use of the identity [Ref. 9, Eq. (2.39)]

$$\frac{dA^z_{\vec{q}_\parallel \to 0,\omega}(z)}{dz} \equiv -\frac{4\pi i}{\omega} \int \frac{dz'\, \partial\sigma^{zz}_{\vec{q}_\parallel \to 0,\omega}(z,z')}{\partial z A^z_{\vec{q}_\parallel \to 0,\omega}(z')}.$$

[13] Equations (2.15) and (2.16) may not look simple, but they are, in that within the long-wavelength expansion, they are essentially *decoupled* equations for $A^z_{\vec{q}_\parallel \omega}(z)$ and $\vec{A}_{\parallel \vec{q}_\parallel \omega}(z)$.

[14] $z \to \pm$"∞" means z becomes large in magnitude compared to the surface thickness while remaining small compared to $q_\perp^{-1}$ and $q_\perp^{T-1}$.

[15] S-polarized light hardly couples to plasmons.

[16] The methods used to solve Eq. (2.34) are described in Ref. 9.

[17] In writing Eq. (2.65), it is assumed that $dq_\perp^T < 1$. For a sufficiently thick film this inequality will clearly not be

satisfied; that is, for a thick enough film, the phase change and damping of a transverse wave as it crosses the film must be taken into account. Thus the results obtained below using Eqs. (2.64) and (2.65) cannot be used in the thick-film limit.

[18]See, e.g., P. J. Feibelman and D. E. Eastman, Phys. Rev. B 10, 4932 (1974).

[19]ψ_f is purely outgoing as $z \to \infty$ (cf., Ref. 17). $V(z)$ is the surface potential barrier; the question of how best to choose $V(z)$ is the subject of Sec. III below. See also, P. J. Feibelman, Phys. Rev. Lett. (to be published).

[20]Since the BPPE phenomena of interest are of first order in the wave vector of the incident transverse wave, it is clearly important to develop a model within which the zero-order effects are treated correctly.

[21]The photoyield depends sensitively on the spatial behavior of the electromagnetic field near a surface. See P. J. Feibelman, Phys. Rev. Lett. 34, 1092 (1975).

[22a]P. Vashishta and K. S. Singwi, Phys. Rev. B 6, 875 (1972).

[b]M. S. Haque and K. L. Kliewer, Phys. Rev. B 7, 2416 (1973); Phys. Rev. Lett. 29, 1461 (1972).

[23]B. Feuerbacher (private communication).

[24]I.e., minus, cf. above.

[25]Indeed in a thin enough film photoabsorption is essentially always followed by photoemission, i.e., the electron whose excitation caused the photon absorption escapes into the vacuum. See also Ref. 21.

[26]N. D. Mermin, Phys. Rev. B 1, 2362 (1970).

[27]B. P. Feuerbacher and W. Steinmann, Optics Commun. 1, 81 (1969).

[28]N. V. Smith and W. E. Spicer, Phys. Rev. 188, 593 (1969); U. S. Whang, E. T. Arakawa, and T. A. Callcott, Phys. Rev. B 6, 2109 (1972).

[29]More to the point, a short-wavelength electromagnetic wave.

[30]For the "experimental $\tau(\omega)$," values of $\tau(\omega)$ used were taken from U. S. Whang *et al*. (Ref. 28) and were scaled appropriately to take account of the difference between real bulk potassium and the free-electron gas with $r_s = 5$ [e.g., $\hbar\omega_p(\mathrm{K}) = 3.9$ eV, while within the $r_s = 5$ free-electron gas one finds $\hbar\omega_p(r_s = 5) = 4.2$ eV].